VUV/EUV Ionising Radiation and Atoms and Ions: Dual Laser Plasma Investigations

E. T. Kennedy, J. T. Costello, J-P. Mosnier and P. van Kampen

National Center for Plasma Science and Technology and School of Physical Sciences,

Dublin City University, Dublin 9, Ireland

Corresponding author: Eugene Kennedy (Fax. No. 353-1-7005384: eugene.kennedy@dcu.ie)

Abstract

The interaction of ionizing radiation with atoms and ions is a key fundamental process. This report concentrates on studies of photoexcitation/photoionisation using laser-produced plasmas as continuum sources and synchronized laser plasma plumes to provide the absorbing atom or ion species. Examples from studies of the interaction of ionizing radiation with atoms and ions ranging from few-electron atomic and ionic systems to the many-electron high atomic number actinides are reviewed and illustrate the advantages and limitations of the Dual Laser Plasma technique.

Keywords: vacuum ultraviolet, extreme ultraviolet, laser plasma, absorption spectra, photoionization, atoms, ions, imaging.

1. Introduction:

The study of the interaction of short wavelength photons (in the vacuum ultraviolet and extreme ultraviolet spectral regions) with atoms and ions is challenging both experimentally and theoretically. At these wavelengths, individual photons have sufficient energy to excite either inner-shell electrons or more than one electron at a time. Experiments provide important data for the interpretation of atomic and ionic processes in laboratory and astrophysical plasmas and for critical comparison with the predictions of the most advanced theoretical calculations. The latter must properly include many-body collective effects if they are to correctly predict the photon-atom or photon-ion interactions in the short wavelength energy regions. The atom is an ideal system for the investigation of such effects because atoms are completely reproducible and the basic Coulombic electromagnetic inter-particle interactions which determine their behaviour, are well known. Photoionisation experiments on ions are particularly difficult due to the requirement of combining sufficiently intense ion beams with appropriately bright short wavelength light sources. The study of photoionization can provide information on the inverse processes of radiative and dielectronic recombination which are of importance in modeling astrophysical and laboratory plasmas. Furthermore, data on singly and multiply charged ions can help scientists understand photon interactions with solids because atoms in a condensed matter matrix often exist in ionic form. Interest in the short wavelength regimes is further stimulated by problems in upper atmospheric physics and chemistry and through recent developments such as CHANDRA, which is providing new astrophysical observations extending through the VUV down into the x-ray region.

1.1 Some early developments

Historically, progress in the experimental study of the interaction of short wavelength photons with atoms or ions has been facilitated by successive improvements in instrumentation and particularly light sources. Pioneering investigations were made by Schumann (1893) through innovations enabling him to reach wavelengths as short as 125nm. These included the building of the first vacuum spectrograph, the use of a fluorite prism as the dispersive element and the introduction of the "Schumann" photographic plate of very low gelatin content. As the dispersion curve of fluorite was not known he was unable to measure the short wavelengths observed. That he had reached wavelengths as short as 125 nm was later realized by Lyman, who was the first to make wavelength measurements in the vacuum ultraviolet. By using a concave diffraction grating in his vacuum spectrograph he was able to place a wavelength scale on Schumann's spectrum, as well as reaching much shorter wavelengths than Schumann who had been limited by the transmission of fluorite. Lyman went on to discover the principal series in hydrogen which bears his name, the first member of which is at 121.6nm. In later work, he observed the principal series of helium, the series limit at 50.4 nm and the continuum beyond the limit and in fact reached wavelengths as short as 25 nm (Lyman 1924, 1928). Another very important early observation was the recording and identification of the helium inter-combination line $1s^2\ ^1S$- $1s2p\ ^3P$, which established the link between the ortho- and para-systems of helium.

A further major step towards reaching shorter wavelengths was made by Millikan and Sawyer (1918) when they used a vacuum spark as a light source. Elements were introduced in the form of solid compounds inserted in holes in the electrodes. With this source Millikan and Bowen (1924) discovered the spectra of many highly stripped atoms and showed that they could be arranged into isoelectronic sequences. The vacuum spark source combined with gratings of good reflectivity enabled them to detect very faint lines and to reach wavelengths as short as 14 nm. These workers used the concave grating in normal incidence mode and consequently extremely shorter wavelengths were not detected due to the rapid fall off in reflectivity with decreasing wavelength. By constructing a grazing incidence concave grating spectrograph, Osgood (1927) observed spectra from ~200 nm down to the K_α x-ray line of carbon at 4.4 nm, thus closing the gap between the x-ray and extreme ultraviolet regions.

By using the vacuum spark source many important advances were made by Edlen and his collaborators, in a long series of studies of the spectra of highly stripped ions (Edlen 1964 and references therein). As a result, the energy levels of many atoms in different stages of ionization were established. The importance of this work was most clearly evidenced when Edlen (1942) was able to show that spectral lines of the solar corona, which had long remained unidentified, were in fact due to transitions occurring between levels in the ground terms of highly stripped atoms. This implied that the sun's corona was at a temperature of the order of a million degrees, which up to then was completely unsuspected. Some of the practical difficulties of the vacuum spark were removed on the introduction of the "sliding spark" in which the breakdown occurred over the surface of an insulator instead of across an initial vacuum. The source was easier to use, required lower potentials and gave better-developed spectra. The ionization stages produced by both sources could be controlled to some extent by varying the inductance in the discharge circuit.

In more recent years many new emission sources have become available. Controlled fusion research has led to the development of a number of large plasma sources, some of which have been exploited as spectroscopic sources (e.g. Gabriel (1970)). From the sixties, Fawcett et al (1966), it was realized that the hot dense plasma formed when a Q-switched laser pulse is focused on a target in vacuum constitutes an extremely versatile spectral line source, allowing systematic studies of high ion stages of almost all elements. Laser produced plasmas (Richardson 2000), which provide laboratory-calibrated spectra, have been used widely to generate data banks enabling the identification of many spectral lines from astrophysical sources including the sun and from fusion plasmas.

The development of a variety of light sources has made it possible to carry out absorption studies over a wide wavelength range. *Absorption* spectroscopy provides access to many atomic and ionic levels, which do not show up in emission spectra. This is particularly true of transitions where the upper level is strongly autoionising such as inner-shell or multiple electron excitations or where photoionisation continua are investigated. Historically the continuous spectrum emitted by a hydrogen discharge was the first to be used as a practical continuum background source for

absorption spectroscopy in the vacuum ultraviolet. Lyman (1924) reported a new continuum source, which enabled observations to be carried out at wavelengths as short as 90 nm. The radiation was produced by a short duration capacitor-discharge through a low-pressure gas contained in a glass capillary of small internal diameter (~1mm). Beutler (1935) carried out a series of important investigations of the absorption spectra of the rare gases using as a background source the Hopfield (1930) continuum of helium, extending from about 60 to 100 nm and found numerous absorption lines attributable to excitation of inner-shell electrons and subject to autoionization phenomena.

Ballofet, Romand and Vodar (1961) developed a source, which became known as the BRV source. Initially, the three electrode device was used as a line source but it was found that if the anode consisted of a high Z material, preferably uranium, and if a circuit of low inductance was used to connect the discharge capacitors to the spark gap, a continuum was emitted, extending from the visible down to the extreme ultraviolet (~8 nm). Garton, Connerade, Mansfield and Wheaton (1969) described the use of such a source in conjunction with a containment device for metal vapours, which enabled them to record absorption spectra of neutral metal atoms over a wide spectral range (12 – 65 nm). Cantu and Tondello (1975) added a narrow capillary made of insulating material to the tip of the anode, forcing the discharge into a definite region and they used a toroidal mirror to focus the continuum onto the slit of a 2m grazing incidence spectrograph. The focusing system was capable of both utilizing the full aperture of the spectrograph and of removing its astigmatism. Spectra suitable for absorption spectroscopy required only a one-shot exposure and extended over the 13 – 50nm spectral range. A disadvantage however was that the capillary had to be replaced after every shot.

1.2. Synchrotron radiation sources

The major energy loss in synchrotrons is due to the emission of radiation as the charged particles undergo centripetal acceleration. Schwinger (1949) made detailed calculations on the energy and spatial distribution of the radiation and showed that for E~1GeV the spectrum extends into the x-ray region. Hartman and Tomboulian (1953) (and Tomboulian and Hartman (1956)) were the first to realize the usefulness of the vacuum ultraviolet continuum produced in this way. In a detailed paper they described their measurements made on the 300 MeV Cornell synchrotron. The importance of the source for absorption spectroscopy was demonstrated by observing the absorption edges of beryllium and aluminum thin films. Some of the attributes of the synchrotron continuum were described by the authors: "its continuous nature, high intensity and wide spectral coverage are attractive features", "the spectral distribution is completely calculable, that is, the radiant energy can be expressed in absolute measure".

In a key paper, Madden and Codling (1963) reported new autoionizing levels in helium, neon and argon recorded in a series of experiments in the 18-47 nm region, using the 180 MeV electron synchrotron at the National Bureau of Standards as a continuum light source. The pioneering results for He provided unambiguous evidence of the breakdown of independent-particle theoretical approaches for the doubly excited states and showed that both electrons must be treated collectively (Cooper et al 1963). Advances in synchrotron radiation sources have since played a key role in further studies of doubly excited helium (Schulz et al 1996) and in double ionization measurements (McGuire et al 1995). Through successive generations of development, synchrotron radiation sources have exploited magnetic wiggler and undulator beam-lines to provide ever more intense photon beams (Weidemann 2003). As the relativistic electron bunches pass through the periodic magnetic fields of the permanent wiggler or undulator magnetic structures they oscillate from side to side and emit more intense and directional photon beams than in the original bending magnet beam-line configurations. Combined with high resolution monochromators, these sources provide the experimentalist with tunable, high intensity, polarized, narrow spectral band-width photon beams which have found numerous applications in biology, condensed matter physics and in the study of the interaction of photons with atoms and ions. Other papers in this issue provide examples of the wide range of results obtained on atoms, ions and molecules, using such large-scale facility synchrotron radiation sources.

Reviews of early developments in VUV/EUV spectrometry include those by Tousey (1962), Garton (1966) and Codling (1973). Excellent descriptions of sources, detectors, short wavelength spectrometers, material properties and experimental procedures for the short wavelength regions, are provided by Samson (1967) and in the recent book edited by Samson and Ederer (2000).

This report concentrates on results obtained using laser-produced plasmas as short wavelength continuum sources and synchronized laser plasma plumes to provide the absorbing atom or ion species. References are included to some results obtained using synchrotron radiation sources so that insight may be obtained on the relative merits of both approaches. Laser plasma based table-top experiments are flexible and have produced a wide range of interesting data (particularly on ions) in their own right and have also provided useful preliminary data for later more detailed experiments at storage ring facilities. The examples in the following sections range from studies of the interaction of ionizing radiation with few electron atomic and ionic systems up to the high atomic number actinides and have been selected to illustrate the advantages and limitations of the DLP technique. The paper concludes with a future perspective, which anticipates the new Free Electron Laser developments that will provide uniquely intense VUV radiation beams and introduce a new era in the study of ionizing photon-atom/ion interactions.

2. The Dual Laser Plasma technique

When a high power laser beam is focused onto a solid target in vacuum, a high temperature, high density, short-lived plasma is formed. For light or medium atomic number targets the emission mainly consists of spectral lines. If however a high atomic number target, such as tungsten or a rare-earth target, is used then a clean relatively uniform continuum is emitted throughout the VUV and EUV spectral regions (Carroll, Kennedy and O'Sullivan 1978, 1980; Carroll and O'Sullivan 1982). This laser plasma continuum is ideal for a wide range of absorption experiments at

short wavelengths. When used as a back-lighter source to a second laser generated plasma which creates the absorbing atomic or ionic species of interest, the combination provides a flexible approach to the study of inner-shell and multiple electron excitations in atoms and ions. The technique, termed the Dual Laser Plasma (DLP) photoabsorption technique, has been used to investigate the VUV/EUV photon interactions in a wide range of atoms and ions. The method is versatile as solid targets are used and even refractory elements can be explored. In particular, trends along isoelectronic and isonuclear sequences can be explored. In its earliest formulations the DLP technique used proportional counter (Carillon et al 1970) or photographic detection (Carroll and Kennedy 1977, Carroll and Costello 1986). Photoelectric detection was introduced by the Padova group of Tondello and co-workers (Jannitti et al1984). The extensive review by Costello et al (1991a) provides details on the early developments of the laser plasma continuum source and the DLP technique. Other short reports include Kennedy et al (1995, 2001).

Many of the results reviewed here were recorded with the DLP facility developed at Dublin City University, (Kennedy et al. 1994). The output of a pulsed Nd:YAG laser (~1J in 10 ns) is focused tightly onto a tungsten surface *in vacuo* to generate the back-lighting plasma source of continuum radiation extending throughout the extreme ultraviolet (EUV) spectral region. A second synchronised laser is used to produce the absorbing plasma situated on the optical axis between the back-lighting plasma and the entrance slit of a spectrometer. Figure 1 shows a schematic diagram of the system. Figure 2 shows a close-up of the twin laser plasma arrangement with the sharply focused laser producing the point-like backlighter plasma and a cylindrically focused laser beam producing the absorbing line plasma. By appropriate choices of target material, position of the absorbing plasma with respect to the optical axis, laser irradiation conditions and inter-plasma time delay the absorbing plasma conditions can be optimized for the atom or ion of interest. The continuum output from the back-lighting plasma is coupled, via a toroidal mirror, into the 10-μm entrance slit of a McPherson 2.2m grazing incidence spectrometer equipped with a 1200 grooves/mm grating (Figure 1). The dispersed spectrum is detected by means of a 40-mm-diameter micro-channel plate detector coupled via a coherent fibre optic bundle to a 1024-pixel photodiode array. The system produces single-shot sensitivity with a spectral energy capture at a particular detector position of ~ 3.5 eV at 30 eV rising to ~ 40 eV at 140 eV. The accuracy of wavelength measurement is estimated to be 0.005 nm for sharp features and the spectral resolving power is of the order of 1400.

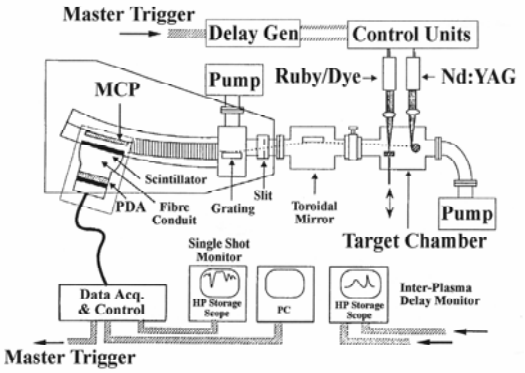

Figure 1. *Schematic diagram of the DLP facility at Dublin City University (Kennedy et al 1994).*

The spectral data are obtained in the following way. By firing the back-lighting Nd:YAG laser alone the background continuum spectrum (I_O) is obtained. By firing both lasers together the transmitted intensity (I) is recorded. EUV emission from the cooler second plasma is negligible so that the quantity Ln (I_O/I) yields the required absorption data. Signal averaging is employed to improve the signal-to-noise ratio of both I_O and I. The inter-plasma delay and laser pulse profiles are monitored on each and every shot to ensure reproducible conditions.

The peak cross sections of atomic spectral features can vary enormously. This provides a severe challenge for the DLP technique, as photoabsorption is an exponential process. In order to observe weak spectral features a high absorbing line density must be used which results in the saturation of strong features. Figure 2 shows how a varying integrated line density can be produced. Using a cylindrical lens to generate the absorbing column and a movable knife-edge to change the effective length of the column, absorption spectra optimized for a range of cross section values can be recorded.

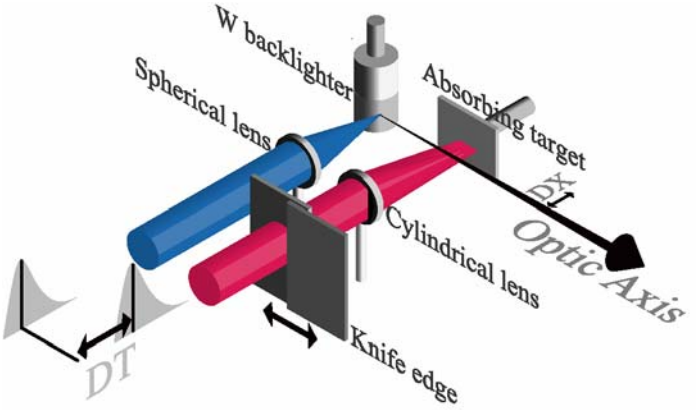

Figure 2. *Detailed schematic of the twin laser plasma configuration used in the DLP technique. DT represents the time delay between the two laser pulses. A cylindrical lens is used to produce the absorbing plasma plume. The length of the absorbing column can be varied by moving micrometer controlled knife edges.*

3. Examples of DLP atomic and ionic data

3.1. Single photon - few electron atom/ion interactions

3.1.1. Photoionisation of Li^+:

Since the sixties, there has been a continued interest in the interaction of ionizing radiation with He, particularly in the photon energy regimes leading to the formation of doubly excited states or to double ionization. Additional experimental difficulties are associated with the observation of comparable processes in helium-like Li^+, as lithium is a metal at room temperature and the photon energies required to produce doubly excited states lie above 150eV. Single electron excitations occur in Rydberg series converging to the single electron ionisation limit at 75.64 eV. Mosnier et al (2000) recently exploited the DLP technique to carry out the first systematic experimental study of the relative photoionization cross-section of Li^+ in its ground state over the photon energy range (60 to 190 eV) extending from the discrete region up to two-and-a-half times the ionisation threshold energy. Figure 3 shows the experimental relative cross-section spectrum. Because of the large variation in the cross section as a function of energy the length of the absorbing plasma plume was varied systematically using the arrangement illustrated in Figure 2 above. For photon energies greater than ~140 eV, correction factors for scattered light contributions to the data were calculated from detailed analyses of the transmission spectra measured using calibrated thin solid films of aluminium or mylar. The associated uncertainties on the relative cross-section measurements were found to be negligible. The cross section shows the first doubly excited state at 150 eV, which is seen to make an almost negligible contribution to the total cross-section due to its very low oscillator strength.

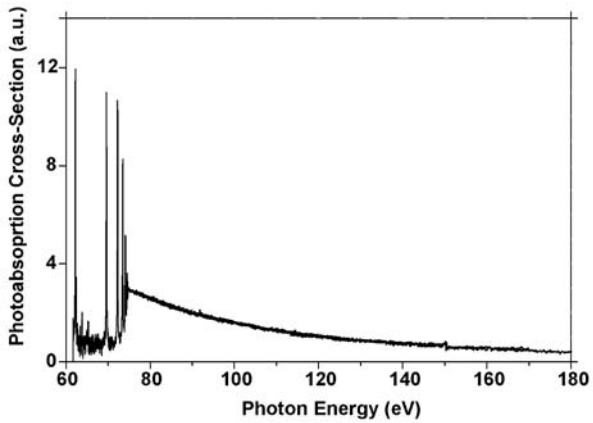

Figure 3. *Experimental relative photoabsorption cross-section of the Li^+ ion, in its ground state, between 60 and 180 eV. The resolved discrete structures between 60 and 75.64 eV correspond to transitions to 1snp excited states with n = 2 to 7. The relative intensities of the first two members at 62.2 and 69.6 eV respectively are distorted by optical saturation effects. Above the threshold energy of 75.64 eV, the photoionization continuum corresponds to transitions to 1sεp continuum states. The 2s2p doubly excited resonance is visible at a photon energy of ~150 eV. (From Mosnier et al 2000)*

The above ionisation threshold experimental results were compared with various Li^+ cross-section calculations and the hydrogenic character of the cross-section behaviour was evaluated. A normalization procedure showed the relative photoionization cross-section data to be consistent with R-matrix calculations in the measured region of the continuous spectrum. The results of other types of calculations were also compared and contrasted with the He case. The Li^+ cross-section was shown to deviate considerably from hydrogenic behaviour despite the increased ionicity.

3.1.2. Doubly-excited states of Li^+.

The first observations of Li^+ doubly excited states produced by photoexcitation were achieved by the DLP technique using photographic detection (Carroll and Kennedy 1977). The lowest-lying doubly excited state for Be^{2+} was similarly recorded in a DLP experiment, by Jannitti et al (1984). Photogeneration of multiply excited states are of particular interest as the incoming photon only interacts directly with a single electron and the formation of doubly or triply excited states relies totally on electron correlation. More recently, as part of an experimental effort to detect triply excited states in neutral lithium (see below), the DLP system with photoelectric detection, as described in section 2, was used for Li^+. The absorbing lithium plasma plume was produced by a ruby laser pulse (30 ns, 1J), which was focused on a solid lithium target in vacuum. The temporal and spatial evolution of Li^+ in the plume was mapped out, with a spatial resolution of the order of 100 μm and a temporal resolution of the order of 20 ns, by measuring the strength of the Li^+ absorption signal, in the singly excited region around 60-70 eV, as a function of space and time in the absorbing lithium plasma plume. This is shown in Fig. 4(a). The population of Li^+ was maximized at a time delay of ~ 100 ns and at a distance of ~ 1 mm from the lithium target surface. Fig. 4(b) shows the photoabsorption spectrum of Li^+ in the 150 eV region, which was recorded under the conditions that maximized the ground state Li^+ absorbing column density as determined from Fig. 4(a). The doubly excited resonance $1s^2(^1S_o)\rightarrow 2s2p(^1P_1)$ is clearly seen. With a spectrometer slit width of 10 μm the best resolution obtained was ~ 1500 (before deconvolution), limited by the spatial sampling period of the array detector. Using a maximum-likelihood procedure the instrumental broadening was removed from the raw spectrum and the Fano resonance parameters were determined (Kiernan et al 1994).

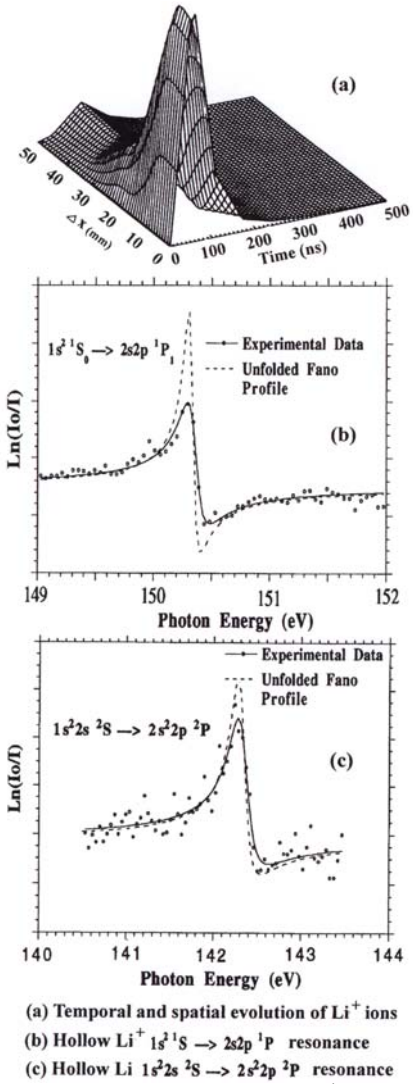

Figure 4. *Photon induced doubly excited hollow Li^+ and triply excited hollow Li.*
(a) Temporal and spatial evolution of Li^+ in a ruby laser-produced lithium plasma: Δx is the spatial position (mm) of the target with respect to the optical axis of the system and time is the inter-laser time delay in nanoseconds (b) The doubly excited Li^+ 2s2p resonance measured at the optimized plasma conditions as determined from (a). (c) Shows the triply excited $2s^2 2p$ resonance of neutral lithium recorded with a dye-laser generated plasma (See text for further details). From Kiernan et al (1994)

3.1.3. Photon-Induced Triply Excited States in Lithium:

Neutral lithium makes possible the formation of triply excited states in which all three electrons are excited leaving the K shell unoccupied. Such triply excited states have been termed hollow atom states and lithium is a model system for the study of electron correlation in a three-electron atom (the Coulombic four-body problem). While helium exhibits only direct double photoionization He+ hf $\rightarrow$ He^{2+} +2e, lithium offers the potential for the study of both direct and resonant (Li+hf $\rightarrow$ Li***$\rightarrow$ Li^{2+} +2e) double photoionization, where Li*** corresponds to a triply excited (or double K-shell vacancy) state. Early observations of lithium triply-excited states were recorded in beam foil or electron impact experiments. Such experiments access a range of hollow atom resonances of differing symmetries but provide little control on their excitation and the many decay channels can make interpretation difficult.

Studies of hollow lithium received a major stimulus from the first DLP photogeneration experiment (Kiernan et al 1994), which provided sufficient resolution to observe the profile of the lowest lying triply-excited resonance and had the advantage of selective excitation. In order to optimize the atomic lithium column density it was necessary to use a long-pulse-duration (~1μs) dye laser as it produced a high density of neutrals. The absorbing neutral lithium column was produced in a 22-mm-long line focus of the dye laser output and maximized by observing the absorption spectrum in the 60 eV photon range. Figure 4(c) shows the resulting $1s^22s^2S\rightarrow 2s^22p\ ^2P$ resonance at 142.3 eV. The broken line represents the Fano fit to the deconvolved data and yielded the energy and shape parameters for the resonance (Kiernan et al 1994). Detailed measurements of the energy, width (Γ) and Fano profile parameter q compared favourably to theoretical predictions available at the time.

The successful observation of the triply excited state $2s^22p$ in neutral lithium illustrates the flexibility of the dual-laser plasma system and is the severest test of its performance to date. Subsequent photoion spectrometry experiments at the HASYLAB (Kiernan et al 1995) and Photon Factory (Azuma et al 1995) storage rings had greater spectral resolution and sensitivity and discovered many new hollow atom resonances at higher photon energies. In these experiments lithium atomic beams were created using furnaces and crossed with the synchrotron radiation photon beams and the resultant ions (Li^+ and/or Li^{++} ions) were detected. It is notable that the width of the $2s^22p\ ^2P$ resonance was overestimated in the DLP experiment. Later experiments on a range of resonances in different atoms and ions show that by recording DLP spectra under different opacity conditions, more accurate measurements of resonance widths may be obtained by extrapolating the measured profile parameters to zero opacity conditions (Gray 1999).

The most recent experiments on hollow lithium, particularly those based on photoelectron spectrometry at the Advanced Light Source (Diehl et al1996), have allowed very weak resonances such as the $2p^3$ state to be investigated in detail. Doubly hollow states (both K and L shells empty) have been observed (Diehl et al 1997a and Azuma et al 1997). Angular resolved measurements have been made on both the $2s^22p$ (Diehl et al 2000a) and $2p^3$ (Diehl et al 2000b) resonances. Extended Rydberg series have also been detected (Diehl et al 1997b). Figure 5 shows members of a Rydberg series of triply excited states recorded via photoelectron spectrometry, where the decay channel selectivity allows the resonances to be clearly observed in the doubly-excited ($2s^2\ ^1S$) decay channels whereas they are barely detectable in the 1s2s ^3S channel. Two-colour experiments in which the selectivity of synchrotron-photon excitation is combined with laser-photon excitation of ground state lithium atoms allow even-parity hollow lithium states to be produced (Cubaynes et al 1996). Decay of triply excited states $Li(nln'l'n''l'')\rightarrow Li^+(\ nln'l') + e^-$, is quickly followed by a further Auger decay $Li^+(\ nln'l')\rightarrow Li^{++}(n=1) + e^-$. By observing the latter decay electrons, which are emitted with definite energies corresponding to the differences between the energies of the Li+ doubly excited states and the energy of the Li^{2+} ground state, detailed information on the positions of the Li^{2+} doubly excited states can be deduced (Diehl et al 1997c, 1999).

Since 1994, prompted by the results from photogeneration experiments, many new advanced calculations on hollow lithium have been carried out (Chung and Gow 1995,1996, Chung 1998, Conneely and Lipsky 2002). The decay patterns of the hollow states have been investigated theoretically in order to understand the physical reasons behind the relative magnitudes of their widths and to guide experimentalists with regard to the best decay channels to study [Chung 1999, Verbockhaven and Hansen 2000). In an analogous way to the treatment of doubly-excited states the use of hyperspherical coordinates and molecular viewpoints are also being developed for the triply-excited lithium system (Clark and Greene 1980, Greene and Clark 1984, Morisihita et al 1997, Morishita and Lin 1999, Grujic 1999). The high number of degrees of freedom makes such calculations a continuing theoretical challenge but should pay the rich dividend of providing key physical insight into triply correlated electron motions. Triply excited lithium is a nice example of a case where the first results, obtained with the DLP method, stimulated many further experiments at large-scale storage ring facilities. For further details and more complete sets of references on the study of triply excited states in lithium see the reviews (Kennedy et al 1998, Wuilleumier et al 1998, Wuilleumier 2000, Kennedy 2001) and the accompanying article by Azuma et al in this special edition.

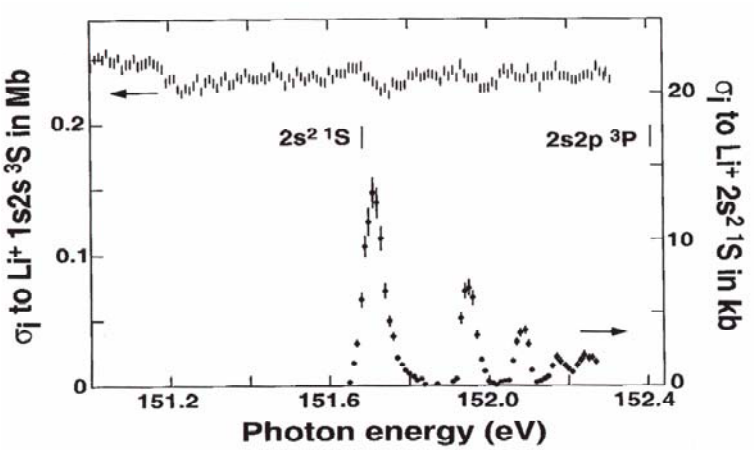

Figure 5. *Rydberg series of triply excited states of Li running to the Li^+ doubly excited limit $2s2p\ ^3P$, observed in electron spectroscopy experiments at the Advanced Light Source storage ring. The measured values of the partial cross sections for photoionization of $1s^22s\ ^2S$ Li atoms into $1s2s\ ^3S$ (upper curve, left scale) and $2s^2\ ^1S$ (lower curve, right scale) Li^+ ionic states, are shown. The resonances are clearly seen in the $2s^2\ ^1S$ channel and are barely detectable in the $1s2s\ ^3S$ channel. See text for further details. (From Diehl et al 1997).*

3.1.4. Triple ionisation of the lithium atom:

The complete photo-disintegration of the lithium atom can occur only by simultaneous ejection of all three electrons. Triple ionisation of lithium therefore constitutes, in a sense, the limit of photoexcitation of the three electrons. In the near threshold behaviour of double and triple ionisation processes, the electrons leave with low kinetic energy and hence electron correlations are expected to be particularly pronounced. For triple ionisation, lithium is the ideal test case as it avoids possible contributions from remaining electrons. Using photoion time-of flight spectroscopy at the Photon Factory, a first successful measurement of the triple ionisation cross section for lithium has recently been made from the threshold at 203 eV to about 450 eV (Wehlitz et al 1998). The measured cross section never exceeded the extremely low value of six barns (Figure 6). Later experiments investigated the near threshold behaviour of the cross section and provided an analysis in terms of a power law (Wehlitz et al 2000). Analogous experiments to those carried out on helium, in which the directions and momenta of the electrons and ion are all measured simultaneously (Rau 1992), remain a challenge for the future.

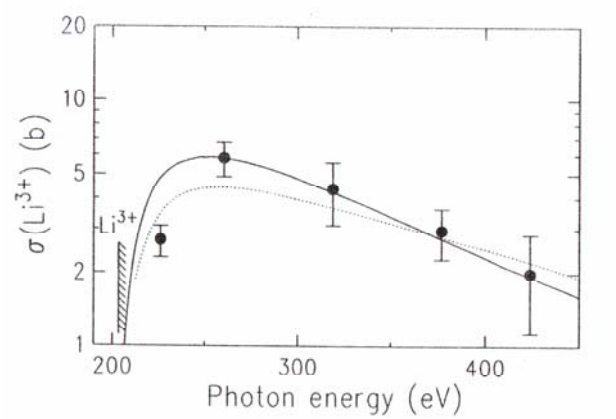

Figure 6. *The absolute triple photoionisation cross section for lithium as measured at the Photon Factory storage ring (From Wehlitz et al 2000). Note the maximum cross section of only six barns.*

3.1.5. C^+ photoionisation:

The Padova group of Tondello, Nicolosi and co-workers have, since the eighties, used the DLP technique with photoelectric detection to investigate the interaction of ionizing radiation with few electron ions of light elements such as carbon (Jannitti et al 1990). For example, the photoionisation cross section of C^+ was measured with the DLP technique by Nicolosi and Villoresi (1998). More recently Recanatini et al (2001) extended considerably the measurements, recording photoabsorption spectra from both the ground $^2P^0$ and the first excited level ^4P. The inter-plasma delay was set at 58ns by an optical delay line. Figure 7 shows the measured absorption coefficient between 40.8 and 57.5 nm, recorded at two different distances (2.1 and 3.3mm) from the graphite target surface, while keeping all other experimental conditions the same. The higher absorption curve corresponds to the higher density close to the target and shows weaker cross section structures more clearly. Both the discrete spectrum and the photoionisation continua were observed. The experiment did not completely isolate C^+ ions and some C^{2+} lines are marked with an asterix on the figure. In order to derive the relative distribution of the oscillator strengths of the discrete transitions and to extend it to the observed continua, a synthetic spectrum was calculated which could be compared to the experimental data. Each spectral line was fitted using Lorentzian profiles of constant width for the various fine structure components and scaling their area according to the relative gf values. An example of the comparison is shown in Figure 8. The fit with the experimental data is seen to be very good and allowed more

accurate definition of the individual resonances and their wavelengths. The work has provided accurate wavelength measurements and new spectral identifications. Relative oscillator strengths were measured and led to f values for several new lines. Photoionisation cross sections from both the ground and the excited states were derived and agree well with calculations and independent measurements. The near-threshold absolute photoionisation cross section for C^+ was recently measured at the Astrid storage ring (Kjeldsen et al 1999a).

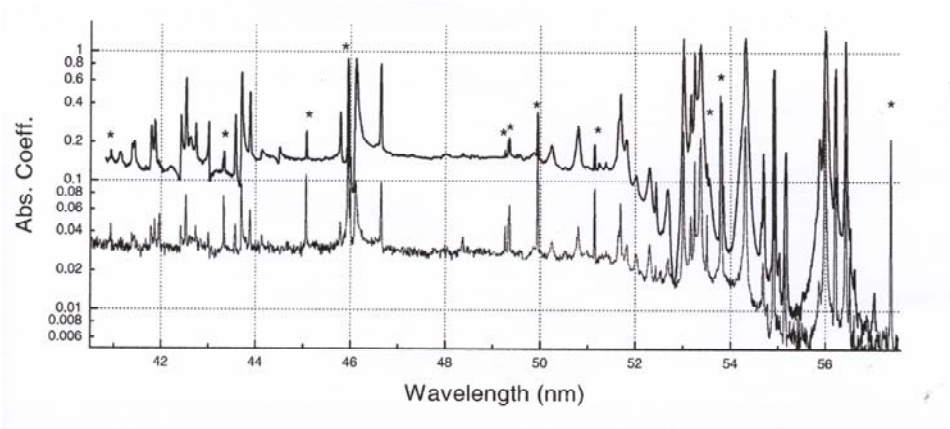

Figure 7. *DLP recorded absorption coefficient spectra of C^+ between 40.8 and 57.5 nm taken at 2.1 mm (top curve) and 3.3 mm (bottom curve) from the surface of the C target. CIII lines are indicated with an asterix. (From Recanatini et al 2001).*

3.2. Inert gas isoelectronic sequences

Rare gases have been extensively studied using synchrotron radiation sources (Schmidt 1997). They are experimentally safe and easy to work with and their closed shell ground state character helps the theoretical interpretation of the data. Detailed electron spectrometry and angular resolved measurements have been made (Schmidt 1997). On the other hand, ions isoelectronic to the rare gases have hardly been studied. In this section, some recent DLP investigations of ions in the neon, argon and krypton sequences are briefly reviewed.

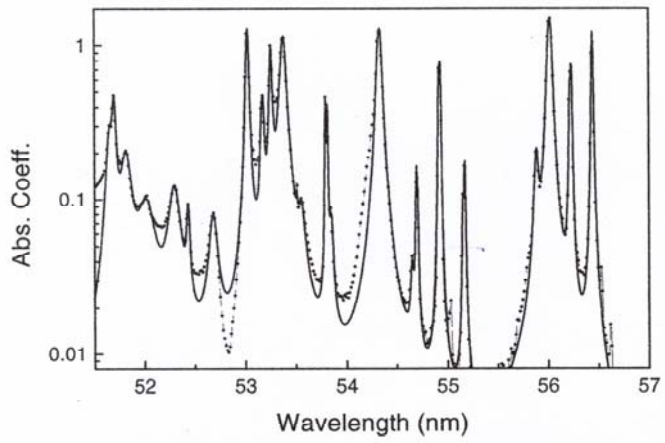

Figure 8. *Synthesis of the C^+ absorption spectrum in the 51.5 – 56.5 nm band. The continuous curve shows the synthetic spectrum; the line-dotted curve shows the experimental spectrum. (From Recanatini et al 2001).*

3.2.1 *The neon isoelectronic sequence:*

The importance of photoabsorption data for ions of the neon sequence, for the determination of radiative opacities for stellar envelopes, was emphasised as part of the Opacity Project by Hibbert and Scott (1994). Members of the sequence considered to be of significant astrophysical abundance include Ne, Na^+, Mg^{2+}, Al^{3+}, Si^{4+}, S^{6+}, Ar^{8+}, Ca^{10+} and Fe^{16+}. The near threshold cross section behaviour for the early members of the neon sequence has been recently examined theoretically and experimentally and demonstrates the importance of including fully the role of inner-shell resonances (Chakraborty et al 1999). The calculations were performed, using the Relativistic Random Phase Approximation plus multi-channel quantum defect theory, for members of the Ne sequence up to Z=100. The seven relativistic single excitation channels arising from the 2s and 2p subshells were included: $2s \rightarrow \varepsilon p_{1/2}$, $\varepsilon p_{3/2}$; $2p_{1/2} \rightarrow \varepsilon s_{1/2}, \varepsilon d_{3/2}$; $2p_{3/2} \rightarrow \varepsilon s_{1/2}, \varepsilon d_{3/2}, \varepsilon d_{5/2}$. The results of the calculations for the cross section at the $2s^2 2p^5\ ^2P_{1/2}$ threshold are shown in Figure 9 (solid points) for the first few members of the sequence. The outstanding feature is the smooth evolution of the cross section along the sequence, with the exception of the Si^{4+} results, which are smaller by more than an order of magnitude. Fig. 9 (continuous line) shows the calculated results with the coupling between 2s and 2p channels omitted, and a marked difference from the full RRPA result is seen. Omitting the coupling essentially excludes the inner shell excitations. Without the coupling, the threshold 2p cross section for Si^{4+} falls into the pattern established by the neighboring members of the isoelectronic sequence, while the other members of the sequence are substantially the same.

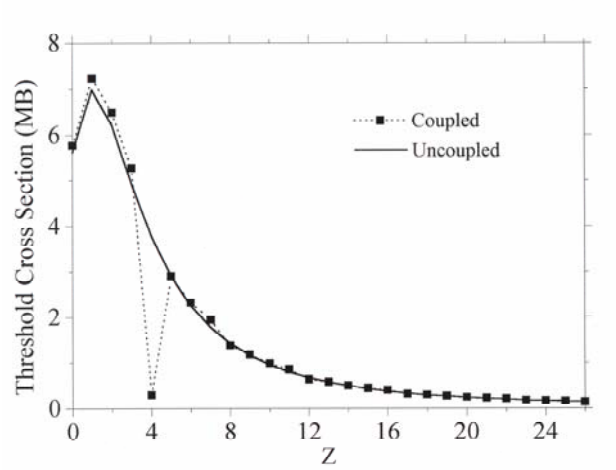

Figure 9. *Calculated photoionization cross section (MB) at the $^2P_{1/2}$ threshold versus initial charge state **z** for the neon isoelectronic sequence. Results are shown with and without inclusion of the coupling between the 2s and 2p channels. (From Chakraborty et al 1999)*

The effects of the inner shell resonances on the calculated cross sections is shown in Fig. 10 for photoionization of Ne, Na^+, Mg^{2+}, Al^{3+}, Si^{4+}, and P^{5+}. For Na^+ the remnants of the *2p* $\rightarrow \varepsilon d$ delayed maximum, evident for neutral neon, is responsible for the slightly increasing cross section at threshold; most of the rise has moved below threshold into the discrete region. Mg^{2+} shows an almost flat cross section with a slight increase well above threshold. The Al^{3+} cross section is virtually flat at threshold but is gradually dominated by the inner-shell *2s* $\rightarrow$*3p* resonance which has moved down in energy to within ~13 eV of the threshold; the analogous resonance in Mg^{2+} explains the slight tailing up of the cross section seen in Fig.10(c). For Si^{4+}, this resonance just straddles the ionization limit, thereby changing the threshold cross section dramatically. For P^{5+}, the *2s*$\rightarrow$*3p* resonance has moved well below the ionization limit and the threshold cross section behavior returns to "normal." However, the *2s*$\rightarrow$4p resonance is now seen to move down into the near-threshold region. The movement of successive inner-shell resonances through the ionization limit evidently occurs along the entire neon sequence. The key, therefore, to the anomalous threshold cross section for Si^{4+} is clearly the fact that the inner shell 2s$\rightarrow$np resonances move towards the discrete region, below the 2p thresholds, with increasing Z along the sequence.

The movement of the inner shell resonance to the vicinity of the threshold region is confirmed by the DLP recorded results for the sequence members Na^+ through Si^{4+}, shown in Figure 11. For the ions Na^+ to Al^{3+} we see the valence transitions (2p$\rightarrow$ns, nd) running to the series limits indicated, with a smooth continuation in the cross section across the limits. For Si^{4+} the behaviour is strikingly different. The near-threshold cross section is now dominated by the inner-shell 2s$\rightarrow$3p resonance which has moved down to just below the ionization limit. The resonance is centered at 165.4 eV, whereas the photoionization limits $^2P_{3/2}$ and $^2P_{1/2}$, as determined from extrapolation of the valence 2p$\rightarrow$ns,nd series, lie at the indicated positions of 166.7 and 167.2 eV, respectively.

As Z $\rightarrow\infty$ for any isoelectronic sequence the 2s and 2p thresholds become degenerate since they have the same principal quantum number. The downward movement of inner-shell resonances with respect to outer-shell thresholds therefore occurs for all sequences for which the outermost subshell is other than l = 0. Whenever an inner-shell resonance, on its downward trek along the sequence, falls in close proximity to an outer threshold, consequent dramatic modification of the near-threshold cross section can result. The results imply that this resonance-induced threshold effect is quite a general phenomenon and interpolation or extrapolation of photoionization and recombination cross sections along sequences should be viewed with extreme caution unless the role of inner-shell transitions is accurately included.

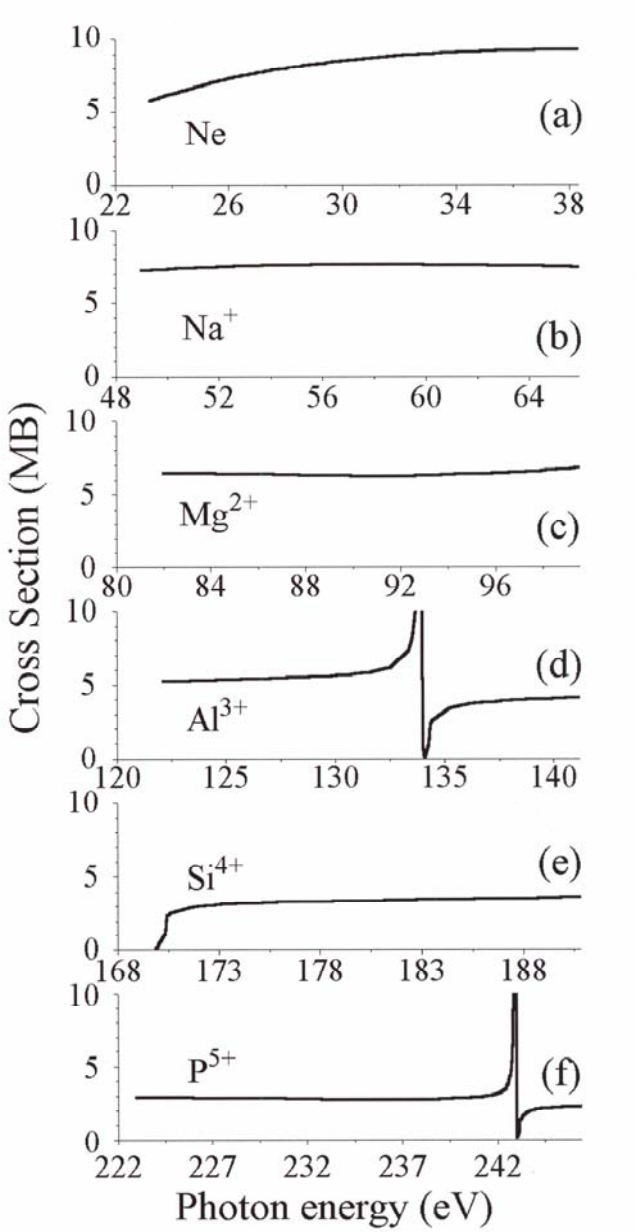

Figure 10. *Calculated near-threshold photoionisation cross sections for (a) Ne, (b) Na^+, (c) Mg^{2+}, (d) Al^{3+}, (e) Si^{4+} and (f) P^{5+}. Note that the full height of the Al^{3+} resonance peak is not shown. (From Chakraborty et al 1999)*

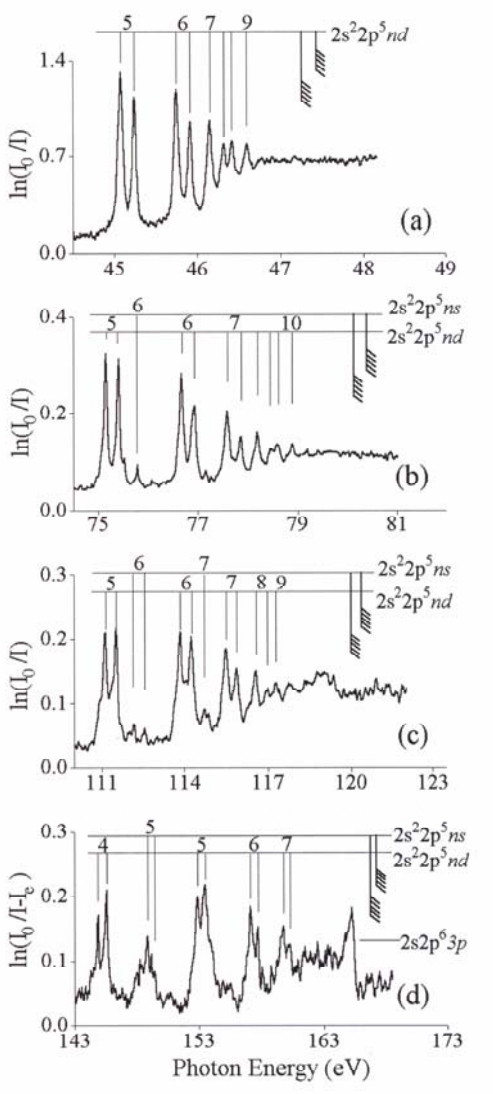

Figure 11. *Experimental photoabsorption spectra for a) Na^+, (b) Mg^{2+}, (c) Al^{3+} and (d) Si^{4+} with many of the $2s^2 2p^5 nl$ absorption features identified. The $2s^2 2p^5\ ^2P_{3/2,1/2}$ thresholds are indicated. Note the changes in the energy scales along the sequence. (From Chakraborty et al 1999)*

3.2.2. The argon isoelectronic system:

Extensive theoretical and synchrotron based experimental investigations have been carried out on argon atoms over many years. For the Ar like ions K^+ and Ca^{2+} however only a few experiments have been carried out. In their pioneering development of the crossed ion and synchrotron radiation beams technique, Peart and Lyon (1987) measured the photoionisation cross section of K^+ in the region of the 3s-subshell excitations. They were, however, unable to examine discrete structures. The DLP technique has been exploited (van Kampen et al 1997) to record the inner shell photoabsorption spectra of K^+ and Ca^{2+} with high enough spectral resolution to examine the resonance structures and the results show that the behavior of the 3s→np resonances differs radically from that in Ar . The 3s→np DLP recorded spectra are shown in Figure 12. On moving from Ar to K^+, a striking q-reversal is observed for the 3s→np transitions, while the resonances maintain a distinct window-like appearance. In Ca^{2+} the main 3s→4p resonance almost disappears and the higher 3s→np resonances have become almost symmetric absorption lines indicating much weaker interactions with their associated εl continua. By applying the RPAE method in conjunction with the Dyson equation method to positive ions for the first time (van Kampen et al 1997), double-electron processes were shown to play a crucial role in the interpretation of the resonance structure. The calculations showed that the changes in profiles are affected by changes in the positions of the 3s and 3p Cooper minima along the sequence. In Ar, all 3s resonances lie below both Cooper minima. In Kr^+ the 3s Cooper minimum lies in the discrete spectrum but the 3p minimum lies above all the resonances; this explains the consistent q parameters and the extreme weakness of the 3s→np transitions. In Ca^{2+}, the 3s Cooper minimum lies below the discrete resonances while the 3p minimum lies just above the 4p resonance, causing a change in the imaginary part of the 3s→4p amplitude and hence in q. Double-electron correlations dramatically affect the Fano parameters for the resonances by changing the locations of the 3s and 3p Cooper minima. In particular, the width of the Ca^{2+} 3s→4p resonance increases and the q-parameter changes sign. The *3s→4p* resonance is very different from the *3s→np* resonances. It is very wide and diffuse and has a *q* value of about -1, while the other resonances are narrow absorption-type features with high q values. For a detailed description of the extensive theoretical calculations used to interpret the experimentally observed behaviour, see van Kampen et al (1997). Lagutin *et al* (1999) have used a different theoretical approach and computed the

cross sections with a configuration-interaction Pauli-Fock (CTPF) method. The results agree very well with experiment and provide an explicit picture of the modulation of the 3s-np resonance structure by the Cooper minimum as it moves through the *3s* threshold with increasing ionization. More recently the K^+ spectrum has been re-examined experimentally using the ion beam facility at the Aarhus storage ring. The DLP results are in reasonable accord with the storage ring data but importantly the latter succeeds in putting the cross section values on an absolute scale (Kjeldsen et al 1999b).

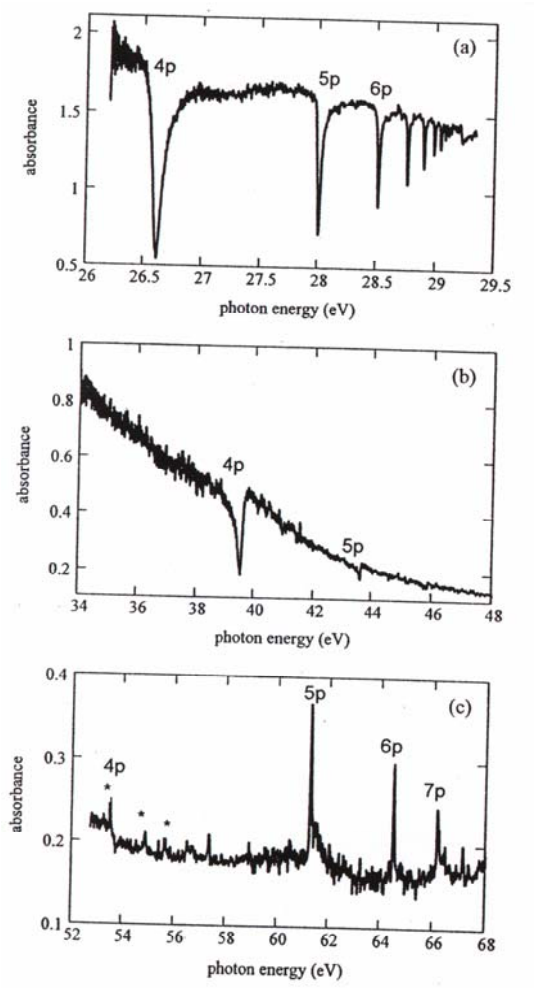

Figure 12. *Experimental 3s→np photoabsorption spectra of (a) Ar, (b) K^+ and (c) Ca^{2+}. (From van Kampen et al 1997)*

3.2.3. The krypton isoelectronic system

DLP experiments have been most recently extended to the next row of the periodic table where the 4s-subshell spectra of Kr- like Rb^+ and Sr^{2+} have been examined (Neogi et al 2003). Figure 13 shows absorption spectra for atomic Kr, Rb^+, and Sr^{2+} in the photon energy range where $4s^14p^6np$ Rydberg and $4p^4n'l'n''l''$ doubly excited resonances appear. The Kr data were taken from Codling and Madden (1972). The DLP recorded Rb^+ and Sr^{2+} spectra display well-developed resonance structures and were obtained by firing the back-lighting continuum pulse at delays of 200 ns and 50 ns after the initiation of the Rb and Sr sample plasmas, respectively. All three spectra are dominated by characteristic asymmetric profiles which vary from window-type resonances with small *q* values of ~0.25 to asymmetric features with moderate values |q| <3. The most striking difference between the neutral Kr atom and the ionized Rb and Sr ion spectra involves the lowest energy resonance structure, which consists of a single feature only for the ions. This is in contrast to the rather complex multiple structure observed in Kr, which is known to arise from strong double excitations that overlay the main 4s-5p resonance.

An integrated program of Configuration-Interaction Pauli-Fock calculations was carried out, which provides a physical interpretation of the measured spectra and is in good agreement with them. Apart from the intrinsic curiosity associated with studying the isoelectronic partners of one of the most investigated atoms in the periodic table (krypton), the sequence is a test case for the effects of increasing ionization on a high-Z closed shell atomic system. The relative roles of relativistic effects and electron correlation determine the characteristic structure and dynamics of the ions. The relative cross sections, extracted from the photoabsorption data, are well reproduced by the theoretical cross sections. Rescaling the Coulomb interaction was needed to better fit the 4s-5p resonance in Sr^{2+}, indicating a breakdown in the efficacy of second-order perturbation theory for this case. The complex doubly excited resonances straddling the first 4s-5p resonance in Kr, and causing the more complicated multiple structure observed in Kr, were found to move to higher photon energies blending with 4s-np resonances, where n ≥ 6. This isolates the 4s-5p resonances in Rb^+ and Sr^{2+}, which can be parametrized by using a Fano formula.

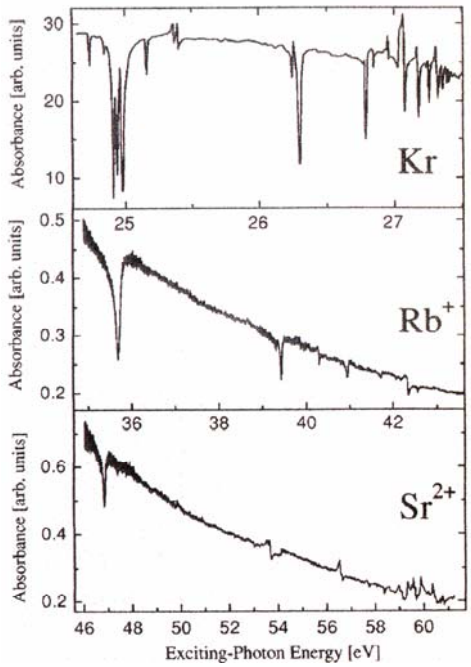

Figure 13. *Experimental photoabsorption spectra of atomic Kr, Rb^+, and Sr^{2+}, in the photon energy range from the 4s →5p Rydberg resonance up to the 4s threshold. The Kr data were taken from Codling and Madden (1972) and the Rb^+, and Sr^{2+} spectra were recorded with the DLP technique (From Neogi et al 2003)*

3.3. DLP investigations of atoms and ions in the 3d and 4d rows

One of the striking features of the photon-atom interaction at short wavelengths is the appearance of broad intense absorption structures, termed 'giant resonances', which are usually related to inner-shell thresholds. Giant resonances are inherently collective phenomena and are of universal interest as they occur in the interaction of VUV photons with atoms, molecules, clusters and solids (Connerade et al 1987). Giant resonances, such as 3p → 3d and 4d → 4f transitions in atoms of the 3d and 4f transition rows of the periodic table, respectively, have been studied extensively through photoabsorption spectroscopy of the 3p subshell and of the 4d subshell (See Mansfield et al 2003 and references therein) From such data it is possible to follow in detail the evolution of the giant resonances along each of these rows. Figure 14 shows, as an example, the DLP recorded spectra in the 3p excitation regions for the elements Cr through nickel (Köble 1994). These illustrate the versatility of the DLP method and the results compare favourably with the spectra previously obtained using synchrotron radiation and furnaces to produce the absorbing vapours.

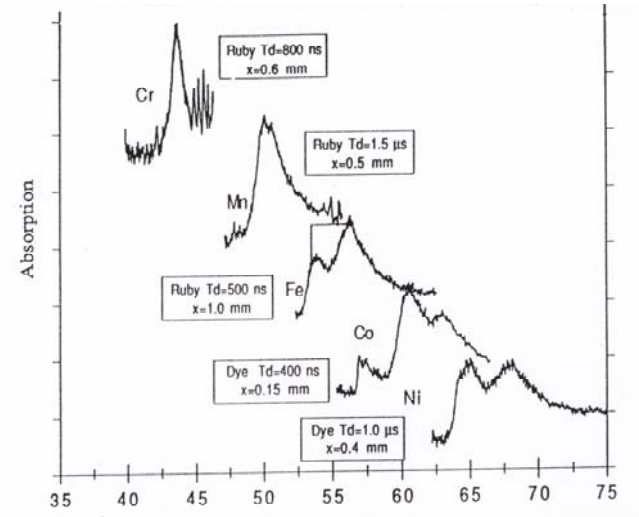

Figure 14. *DLP recorded photoabsorption spectra, in the region of the 3p-3d giant resonance, along the neutral sequence from chromium to nickel. The spectra are displaced vertically for clarity. The laser type, inter-plasma time delay Td and position from the target surface x, are displayed for each spectrum. (From Köble 1994).*

3.3.1. XUV photoabsorption spectra of the zinc isonuclear sequence in the region of 3p-subshell excitation"

The first transition group, extending from Sc to Zn has provided a considerable challenge to theory and experiment, in the energy region corresponding to inner-shell excitation (Sonntag and Zimmermann 1992 and references therein). Apart from chromium $[Ar]3d^5 4s$ and copper $[Ar]3d^{10}4s$, this group of elements is characterized by the successive filling up of the 3d shell. Zinc is the last member of the series and has a closed-shell configuration $[Ar]3d^{10}4s^2$. Using

the DLP technique (Kiernan et al 1997) experimental photoabsorption results were obtained for Zn I, II, III and IV in the energy region corresponding to 3p-subshell excitation (Figure 15: Upper panel). The purity of the spectra was enhanced by the fact that the valence and subvalence excited states of each ion stage lie well above their respective ground states. The spectra ranged from the relatively weak and simple closed 4s-shell system of Zn I to the strong and complex open 3d-shell transition-metal-like Zn IV. Differences in the interaction between the discrete transitions from the 3p-shell, of the type $3p \rightarrow ns$, nd, and the 3d continua, produced by the direct photoionization process, $3d^n \rightarrow 3d^{n-1}\varepsilon f$, are responsible for the variation in symmetry of the resonance profiles. The widths can be understood as the result of various autoionization decay channels, most notably where electron-hole recombination in the 3p level results in the removal of a 3d electron. For the four ion stages, Cowan code (Cowan 1981) calculations were performed and the main identified resonances are shown in the lower panel of Figure 15 for comparison with the experimental results.

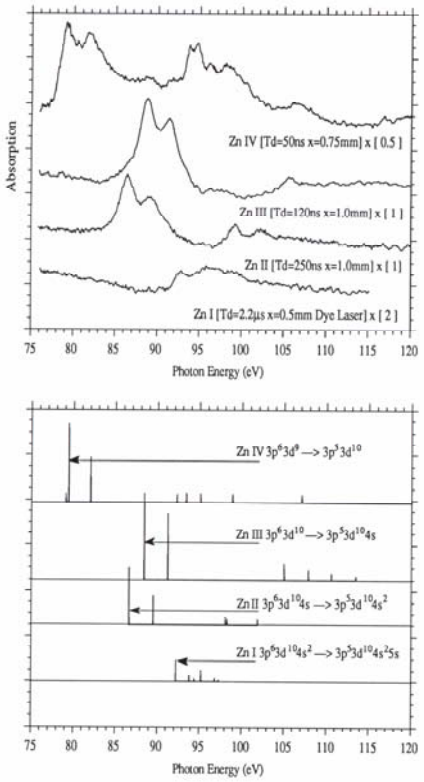

Figure15. *The upper panel shows a summary of the photoabsorption spectra of Zn, Zn^+, Zn^{2+} and Zn^{3+}, indicating the optimised DLP conditions. The lower panel shows the results of corresponding Hartree-Fock calculations, which were shifted by 2.9 eV to lower energy. The calculated data was normalised to the amplitude of the strongest resonance, for each ion stage, in the experimental data. (From Kiernan et al 1997)*

The neutral zinc spectrum was initially optimised in the energy region corresponding to 3s excitation (Connerade and Mansfield 1974) and the spectrometer was then reset to the energy region where 3p excitations were predicted to occur. Using a flashlamp pumped dye laser and a line focus configuration, an absorbing column length of approximately 15 mm was produced and the absorption spectrum in the lower curve of the upper panel of figure 15 was recorded. The experimental data show, as expected, some weak modulations superimposed on the continuous 3d absorption background. Super Coster-Kronig decay processes broaden the 3p core-excited states which form a series of overlapping levels running up to two closely spaced limits $^2P_{3/2}$ and $^2P_{1/2}$ of Zn II at 96.1 and 98.9 eV (Adam et al 1994). Dunne *el al* (1993) later used the DLP technique to photographically measure the 3p photoabsorption spectrum of the isoelectronic Ga^+ ion. The averaged densitometer traces of the plates show reasonable correspondence, in terms of overall spectra signature, with the results for zinc.

For Zn^+ the first allowed transition is to the 4s level and the spectrum shows a significant increase in oscillator strength for the resonance transition 3p —> *4s,* which is composed of two peaks due to spin-orbit interaction within the excited-state configuration. To create the absorbing column of Zn^+, a Q-switched ruby laser was used and the plasma observation conditions were optimized to T_d = 250 ns and x = 1.0 mm. Interaction between the 3p —> 4s discrete transition and the 3d → f continuum in Zn II, is weaker than that between the 3p —> 3d resonance and 3d continuum in the open 3d-shell transition metals, where this interference in the cross section can give rise to asymmetric line shapes. This results in a more symmetric-type profile superimposed on the monotonically decreasing background of the 3d continuum. For Zn II the main resonance profiles could be described by two Lorentzian curves positioned at 86.45 and 89.27 eV, of FWHM 1.9 and 2.1 eV respectively, sitting on a monotonically decreasing background. Good agreement was observed between the calculated and experimental values for the spin-orbit splitting of the resonance. The ratio of the oscillator strengths between the $^2P_{3/2}$, $^2P_{1,2}$ components was calculated to be close to the statistically weighted ratio of 2:1. From the experimental data, the ratio of the areas of the peaks is 0.60 and is, therefore, in reasonable agreement with the calculated ratio.

Doubly ionized zinc has again a closed-shell configuration of $3p^6 3d^{10}\ ^1S_o$, as both of the 4s valence electrons have been removed. The Cowan code calculations predicted that the onset of 3p absorption in Zn III, $3p^6 3d^{10}\ ^1So \rightarrow 3p^5(^2P_{3/2})3d^{10}4s$ should be approximately 2 eV above the onset in Zn II, with respect to their ground states, and that the splitting between the $^2P_{3/2}$ and $^2P_{1/2}$ components should be 2.8 eV. The plasma conditions in the absorbing column, using the ruby laser, were set to T_d = 120 ns and x = 1.0 mm and the absorption spectrum of Zn III was recorded: see figure 8. The two main peaks could be described by Lorentzian curves superimposed on a monotonically decreasing background.

Triply ionized zinc is particularly notable as the vacancy in the 3d shell leads to the fact that a large fraction of the oscillator strength is concentrated in the $3p^6 3d^n \rightarrow 3p^5 3d^{n+1}$ transitions. These discrete states readily autoionize into the $3\ p^6 3d^{n-l}\varepsilon f$ continuum channel. Interaction between the 3p → 3d core-excited resonances and the underlying direct photoionization continua of the 3d-shell produces broad asymmetric-type resonance profiles. The uppermost curve in figure 4 was produced using a tightly focused ruby laser, T_d = 50 ns and x = 0.75 mm, to generate the Zn^{3+} absorption column. The Cowan code *ab initio* calculations predicted the onset of absorption from 3p → 3d for Zn IV to occur about 9 eV below the energy position of the 3p → *4s* resonance in Zn III, relative to their respective ground states, and that the oscillator strength associated with these transitions should be dramatically larger with the opening of the 3d shell.

3.3.2. 4p excitations in Mo^+:

For the transition row elements, high temperatures are needed to obtain significant vapour pressures and the furnace materials are not usually able to withstand chemical attack by the hot metal vapours. In consequence only one 4p-subshell spectrum of an element of the 4d transition row, that of Y I (Z = 39) (Mansfield and Audley 2003) has been recorded using such a method. In a recent paper (Mansfield et al 2003), the dual laser plasma technique has been applied to molybdenum and provides, for the first time, photoabsorption results arising from excitation of the 4p-subshell of Mo^+ ions.

In the DLP experiments, the target material for the absorbing plasma was spectroscopically pure molybdenum and the inter-plasma time delay was varied between 50 and 950 ns. At a time delay of 50 ns the average absorbance was high and was dominated by a continuum background with many superimposed discrete structures. For a longer time delay of 140 ns many strong resonances, associated with higher stages of ionization, disappeared and a marked change in the slope of the overall spectrum was accompanied by the appearance of new discrete resonances. This latter behaviour was further evidenced at a longer time delay of 300 ns and the spectral pattern then remained consistent for further increasing time delays ranging up to 950 ns. For time delays greater than about 500 ns, the overall absorbance became very small as the absorbing plasma expanded and the resulting absorption reduced. The consistent behaviour of the observed spectrum over a wide range of time delays suggested that the observed spectral features are due to the same ionization stage, with little or no contamination from other stages.

Figure 16 reproduces the overall absorption spectrum between 200 000 cm^{-1} (26 eV) and 500 000 cm^{-1} (62 eV) recorded at the optimized time delay of 350 ns, which provided a compromise in terms of time delay, absorbance, and consistent spectral behaviour. The spectrum has been interpreted as due to Mo^+ consisting of a 4p → 4d giant resonance on which extensive discrete structure is superposed (figure 16). With only one exception the discrete lines could be ordered into six Rydberg series, $4p^6 4d^5\ ^6S_{5/2} \rightarrow 4p^5(4d^5\ ^6S)\ (^7P)$ ns,nd (J = 3/2,5/2,7/2), converging on three limits, the Mo III levels $4p^5(4d^5\ ^6S)^7P_{4,3,2}$ (See Figure 17). The ground configuration of Mo II is the half-filled subshell $4d^5$ .The relative simplicity of the observed Mo II spectrum can be attributed to the stable nature of this configuration. The five 4d electrons couple with their spins parallel in the ground state and retain this alignment when the 4p subshell is excited.

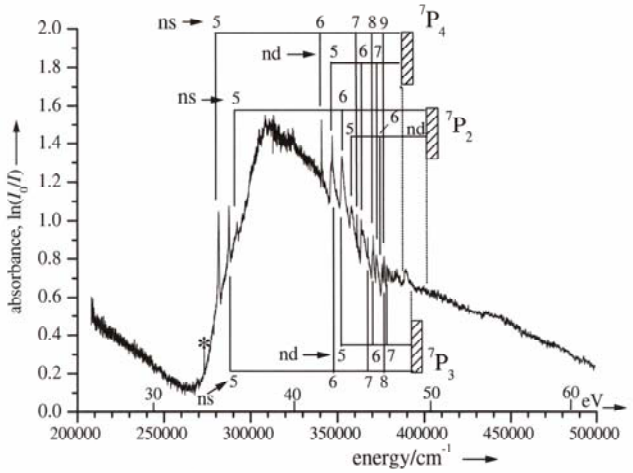

Figure 16. *The Mo^+ absorption spectrum versus photon energy. See the text for further details. (From Mansfield et al 2003).*

Rydberg formulae could be fitted to the series only if (Z -N +1) =2 (corresponding to singly charged ions), where Z is the atomic number and N is the number of electrons in the atom or ion. For the neutral atom the energy spread of the Rydberg series would be less than half that observed. The identification of the spectrum with Mo^+ was reinforced by comparisons between the observed spectrum and the calculated spectra of Mo II and Mo I. In order to take account of the possibility that some contributions to the spectrum may come from either ground or excited state neutral molybdenum or excited states of Mo^+, the observed spectrum was compared with both HXR (Hartree plus exchange with relativistic corrections) and RTLDA (relativistic time-dependent local density approximation) calculations. The detailed analysis indicated strongly that the spectator model of 4p excitation is appropriate and enabled at least 32 new Mo II energy levels to be identified, together with three new Mo III energy levels, which serve as limits for the Mo II Rydberg series. While the calculated line energies generally matched observation well, predictions of line strengths were less impressive. Furthermore the HXR calculations tended to predict a more complex spectrum than was observed, with calculated oscillator strength distributed between more transitions than are evident in the observed spectrum.

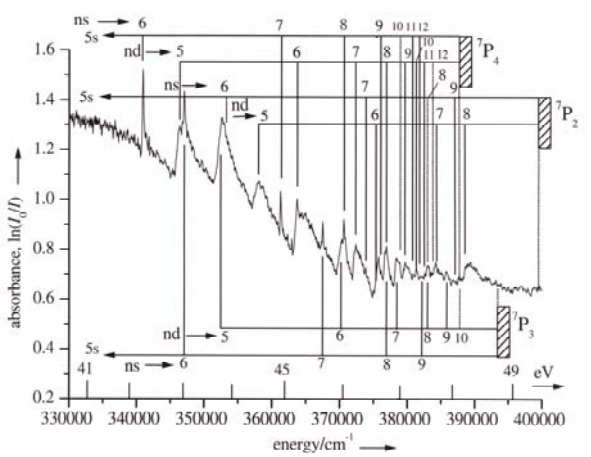

Figure 17. *The Mo^+ absorption spectrum showing higher members of Rydberg series converging on the Mo^{2+} levels $4p^5(4d^5\ ^6S)\ ^7P_{4,3,2}$ levels. (From Mansfield et al 2003).*

An interesting feature of the Mo^+ spectrum is that it displays Rydberg series straddling a giant resonance. The observed asymmetric profiles of the discrete lines (See Figure 16) indicate clearly that they interact with the giant resonance. In particular the reversal of the sign of q (the profile index) as the series passes through the giant resonance is as predicted by Connerade and Lane (1987). This interference effect provides further evidence that the observed giant resonance is also substantially due to Mo^+.

3.4. Evolution of giant 4d resonances in the lanthanides

Giant resonance structures associated with 4d excitations are seen throughout the lanthanides, Figure 18 shows DLP recorded absorption spectra for the elements barium through europium (Köble 1994), which demonstrates the move to higher photon energies as the atomic number increases. Trends in the behaviour of the giant resonances along isonuclear and isoelectronic sequences have attracted considerable theoretical interest. In particular the elements barium and lanthanum have been investigated.

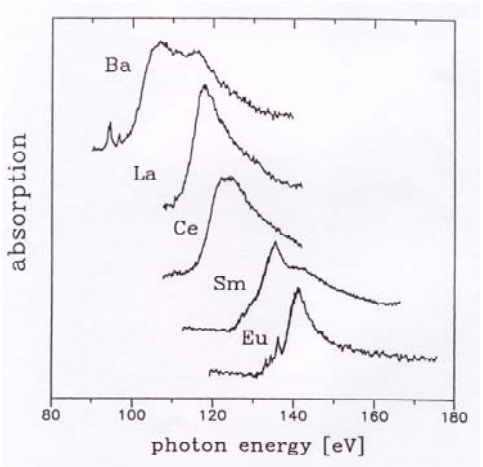

Figure 18. *DLP recorded photoabsorption spectra, in the region of the 4d giant resonance, along the lanthanide neutral sequence from barium to europium. The spectra are displaced vertically for clarity. (From Köble 1994).*

3.4.1. 4d giant resonance evolution between Ba^{2+} and La^{3+}:

In the nineteen eighties, the Resonant Laser Driven Ionisation (RLDI) technique was used to investigate the evolution of the 4d-4f giant resonance in the isonuclear sequence Ba, Ba^+ and Ba^{++} (Lucatorto et al 1981). In RLDI, a tuned

dye laser is used to pump a resonance line of neutral atoms produced in a heat-pipe. Under appropriate experimental conditions this leads to ionization and the production of a Ba^{+} absorbing column. A second dye laser now tuned to a resonance of Ba^{+} leads to a further ionization step and the formation of a Ba^{2+} column. In the experiments by Lucatorto et al, Ba, Ba^{+} and Ba^{2+}columns were separately back-lit with a continuum source and the absorption spectra were registered photographically. A dramatic change in the photoabsorption behaviour in moving from Ba^{+} to Ba^{2+} was observed. This led to considerable discussion in the literature (see Connerade et al 1987 and contributions therein). Further calculations for ions in the XeI isolectronic sequence (Cheng and Froese Fischer 1983; Cheng and Johnson 1983) predicted that in moving from Ba^{2+} to La^{3+}, the $4d^{9}4f(^{1}P)$ resonance should become the dominant photoabsorption feature. Because it does not depend on the tuning of dye laser radiation to resonant transitions, it was possible to use the DLP technique (Köble et al 1995a) to investigate the change in the 4d excitation behaviour between Ba^{2+} and its isoelectronic partner La^{3+} (Figure 19). The photoelectric based photoabsorption cross section data for Ba^{2+} and La^{3+}, enabled a critical comparison between experimental results and predictions based on configuration interaction Hartee-Fock (CI-HF) and many body perturbation techniques. The calculations showed that the giant dipole resonance in La^{3+} associated with the 4d subshell excitation has acquired a definite discrete $4d^{10} \rightarrow 4d^{9}4f(^{1}P)$ character at the expense of the $4d^{10}$ —> $4d^{9}$ef continuum transitions. Polarization effects, revealed through a large term dependence of the $4f(^{1}P)$ state, were found to be strong. Comparison with the corresponding spectrum of Ba^{2+} confirmed the theory, which predicts that the collapse of the $4f^{1}P$ orbital along the XeI sequence has a gradual nature and is not yet complete for Ba^{2+}. Most impressive for La^{3+} is the strong and broad resonance at the photon energy 118-9 eV and the further reduction in the continuum absorption background, when compared to Ba^{2+}.

Apart from their fundamental theoretical interest, photoabsorption cross sections of free ions also provide data useful for the understanding of the electronic structure of solids and molecules. In Figure 19, the corresponding photoabsorption cross sections of solid LaF_3 (Olsen and Lynch 1982) can be compared. Both the La^{3+} and the solid LaF_3 spectra show the dominant $4d^{9}4f(^{1}P)$ resonance and the weak $4f(^{3}D)$ line at about 102 eV. The shoulder at 118.8 eV in the solid state spectrum corresponds to the $4d^{9}_{(3/2)}6p_{(1/2)}$ state in La^{3+}. The comparison shows that the $4f(^{1}P)$ resonance of La^{3+} in its solid state is influenced albeit moderately by the environment, which causes the resonance to be broadened and shifted by about 1.3 eV toward lower energy. The 4d excitations into higher levels are also recognizable in the LaF_3 spectrum. The disappearance of the pronounced line structure that prevails in the free ion spectrum is an indication of the non-localized character of these states. Further details of the experiment and interpretation can be seen in Köble et al (1995a).

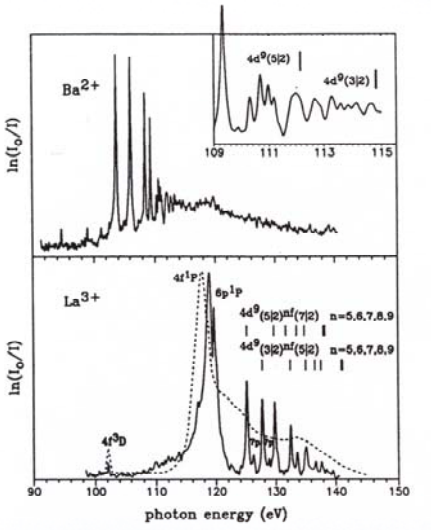

Figure 19. *Photoabsorption spectra of Ba^{2+} and La^{3+} in the 4d excitation region using the dual-laser plasma (DLP) technique. The enlarged Ba^{2+} spectrum shows the $4d^{9}_{(5/2),3/2)}nf$ Rydberg series for n = 9m ...., 12, where the states with the $4d^{9}_{(3/2)}$ hole lie above the $4d^{9}_{(5/2)}$ threshold. The thresholds deduced from the experimental data are 112.2 $\pm$ 0.2 and 114.8 $\pm$ 0.2 eV. The La^{3+} spectrum is shown together with photoabsorption data of solid LaF_3 (dashed curve) from Olsen and Lynch (1982). The thresholds $4d^{9}_{(5/2.(3/2)}$ deduced from the experimental data of La^{3+} are 138.2 $\pm$ 0.2 and 141.1 $\pm$ 0.2 eV. (From Köble et al 1995a)*

3.5. Photoabsorption from excited states

A laser-produced plasma is a complex medium involving many collisional and recombination processes resulting in a spatially and temporally evolving distribution of ions among different ionisation states and excitation levels. For atoms or ions with excited levels energetically well above the corresponding ground states it is generally possible to achieve satisfactory separation of the various ion stages by using the expansion properties of the plasma. It is this temporal and spatial behaviour that is exploited in the DLP technique. Many atoms and ions however have relatively low-lying excited states, some of which may be metastable, and a clear separation is not generally achievable in these cases. The population of excited states can be a useful attribute as it may be used to access different parity autoionising upper states via photoabsorption, which would not be possible from the ground state due to optical selection rules. For example, even-parity autoionising states belonging to the $2p^{5}3s^{2}3p$ configurations of Mg, Al^{+} and Si^{2+} were observed in photoabsorption in laser plasmas deliberately optimised for populations of the $2p^{6}3s3p$ excited states (Mosnier et al 1994). In general however, the presence of substantial populations of excited states is undesirable as

it makes it difficult to separate the individual contributions to the overall plasma absorption spectrum and therefore to deduce the individual relative cross sections. While this situation complicates analysis, it is possible to simulate and interpret the experimental data by superposition of calculated cross sections for the different possible contributing levels weighted according to, for example, a Boltzmann distribution of populations. Recent DLP investigations on chromium ions illustrate this approach. It is worth noting that such computed (and observed) spectra are likely to bear greater resemblance to other laboratory or astrophysical plasma spectra than a simple isolated atom/ion level spectrum. Metastable states also play a role in synchrotron radiation based experiments on ions and have to be taken into account when calculating absolute cross sections (West 2001).

3.5.1. 3p excitations in singly and doubly ionized chromium:

Members of the iron group of the transition elements play an important role in astrophysics. Often termed the 3d elements, they are among the most abundant in nature and are used in many industrial alloys. They have useful magnetic properties and also form the basis for many solid-state laser materials. Because of their widespread relevance the 3d elements have been the subject of many intensive investigations, both experimental and theoretical.

The spectrum of singly ionized chromium was first studied by Costello et al (1991b) using the DLP technique, in the photon energy range 35-70 eV. This energy region is dominated by photoabsorption from the 3p subshell. In singly ionized chromium, with ground state $3d^5\ ^6S_{5/2}$, discrete structures due to 3p→4s excitations were identified, while a broad dominating resonance was ascribed to 3p→3d excitations. Further discrete excitations within this broad resonance were identified by comparison with multi-configurational Hartree-Fock (MCHF) calculations and assigned to 3p→5s, 6s transitions. Subsequent to the experimental investigations, Dolmatov used the spin-polarised RPAE(SPRPAE) technique to compute the Cr^+ photoionisation cross section (Dolmatov 1996). Although he found good agreement with experiment at low photon energies, where 3p→4s transitions and the onset of the 3p→3d giant resonance dominate, serious disagreement with increasing photon energy was evident. This discrepancy was later confirmed by R-matrix calculations of Donnelly el al (1997), which showed a very similar trend.

To understand the discrepancy between theory and experiment a new series of DLP experiments was carried out and supplemented by a series of calculations aimed at assessing possible contributions to the measured absorption by excited states within the plasma (McGuinness et al 1999). The nearest metastable state to the ground state of singly ionized chromium, the $3d^4(^5D)4s\ ^6D$ multiplet, lies only 1.5 eV above the $3d^5\ ^6S$ ground state. Contributions to the observed spectrum due to photoabsorption from these levels may therefore be expected. Recent DLP experiments on singly and doubly ionized chromium ions confirm that excited states play an important role in determining the observed spectra.

The original Cr^+ DLP experiments were carried out at NIST using a long pulse flashlamp pumped dye laser pulse (~1J in 1μs) to create the absorbing chromium plume (Costello et al 1991b). The second series of experiments was carried out at DCU using the DLP set-up described in section 2 above (McGuinness et al 1999). In this case a Nd:YAG laser pulse (~0.8J in 10ns) was used to create the chromium plasma and an extensive range of inter-plasma delays and different spatial regions was investigated together with variations in the on-target laser power density, in order to study any effects these had on the recorded absorption spectrum. It was not possible to obtain a spectrum similar to those calculated by Dolmatov and Donnelly et al for a pure Cr^+ ground state. Furthermore, the observed spectrum, although broadly very similar to that recorded earlier despite the use of a very different performance dye laser, did show variations, particularly above 45 eV, where the main discrepancy with the calculations existed. This suggested strongly that the DLP experiment had not succeeded in isolating ground state Cr^+ ions and that the role of excited states must be included in an interpretation of the experimental data.

To verify the contribution of excited Cr^+ states, the 3p spectra of both ground state ($3d^5\ ^6S$) and metastable ($3d^4 4s\ ^6D$) states were computed. The photoionization cross sections were calculated using the Cowan code (Cowan 1981) in the HFR approximation. Configuration interaction was included for all initial states and for all discrete final states. An ab initio Cowan code calculation did not reproduce well the energies of either the $3p^6 3d^4 4s$ configurations or the $3p^5 3d^6$ configurations. Following the prescription of Cowan, the Slater integrals were reduced from their ab initio values. Even then, small corrections to the calculated E_{av} were required to make the $3d^4 4s^1\ ^6D$ and ^4D energy levels agree better with experiment. An additional correction to the E_{av} of the $3p^5 3d^6$ configuration was also introduced to shift the main 3p→3d peak into coincidence with the earlier SPRPAE and R-matrix theoretical calculations. Cross sections were obtained from the calculated transition energies, oscillator strengths and autoionization decay widths by assuming a Lorentzian profile for each transition. Shown in figure 20 are the resultant individual cross sections calculated using the CI method from the $3d^5\ ^6S_{5/2}$ state and the levels of the $3d^4 4s\ ^6D$ manifold. The calculations show that 3p→3d photoabsorption from the $3d^4 4s\ ^6D$ levels largely occurs above 45 eV. A simulated experimental photoabsorption spectrum was calculated by taking a weighted sum over the ground and metastable states, with the assumption of a Boltzmann distribution of level populations. Calculated photoabsorption spectra were calculated for a variety of temperatures ranging from 0 to 3 eV. For low temperatures, only the ground state is important and the calculated cross section looks similar to the calculations of Dolmatov (1996) and Donnelly et al (1997); see the $3d^5\ ^6S_{5/2}$ spectrum in figure 20. Increasing the temperature yielded larger contributions from the higher lying metastable states and a rapidly decreasing intensity of the sharp 4s lines, bringing the calculated spectrum more into line with the observed spectrum.

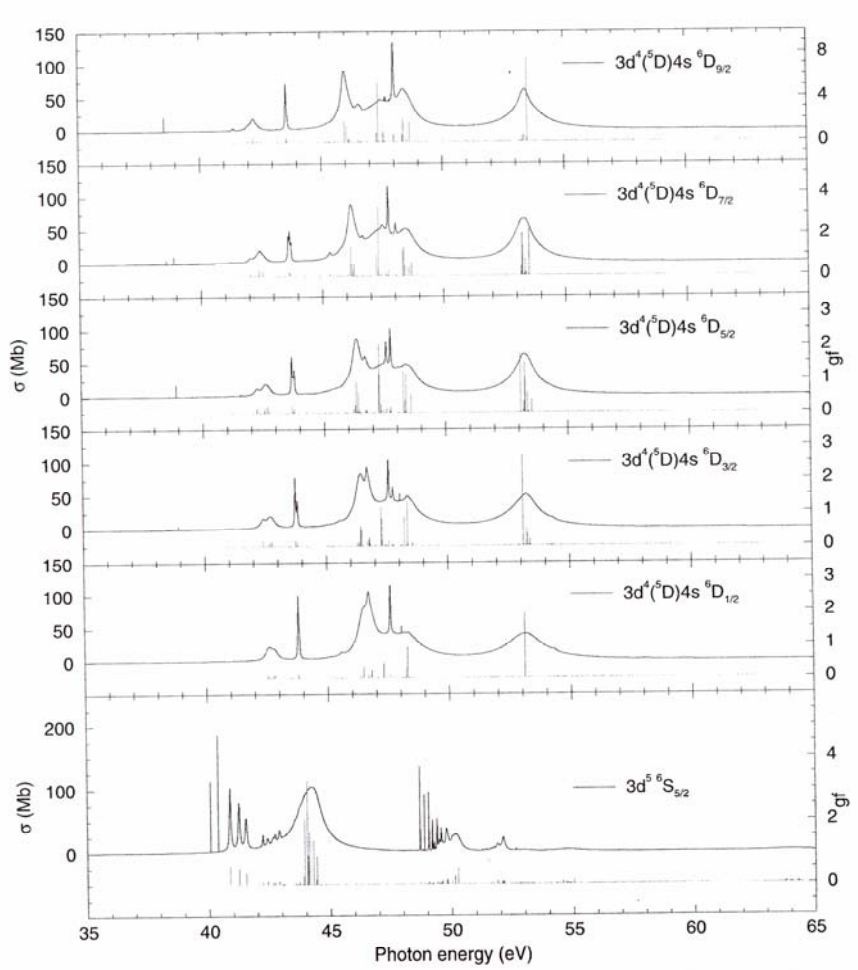

Figure 20. *Calculated 3p photoabsorption cross sections from Cr^{+} $3d^5\ ^6S_{5/2}$ and $3d^4 4s^1\ ^6D$ levels. Shown are the calculated photoabsorption cross section (full curve) and the gf-values of the calculated transitions. (From McGuinness et al 1999)*

In comparing recent DLP data for Cr^{2+} ions with theory, synthetic spectra based on a mix of ground state and excited state ions again resulted in providing reasonable agreement with the observed spectra (McGuinness et al 2000). The relevant plasma temperature and ionization balance were obtained from simple analytical models for various times during the expansion phase of the plasma plume. Experimental spectra taken at different time delays compared well with Cr^{2+} spectra computed for corresponding predicted temperatures. It was found that in order to produce synthetic spectra that matched experiment well, it was necessary to take into account absorption from many states belonging to the Cr^{2+} ground state configuration $3p^6 3d^4$, while states from the nearest metastable configuration $3p^6 3p^3 4s$ make a negligible contribution.

Further details on the Cr^{+} and Cr^{2+} experiments and the extensive series of supporting calculations are provided in the original publications (McGuinness et al 1999, 2000).

3.6. Photoabsorption of heavy elements

Because the absorbing species is created by intense laser interaction with solid targets, it has proved possible to apply the DLP technique to a number of high atomic number (and often refractory) elements such as tungsten, platinum, gold, thorium and uranium.

3.6.1. XUV photoabsorption of laser-generated W and Pt vapours:

In the 5d metal series, overlaps of the 5p and 5d orbitals produce strong correlation effects. The relative positions of the 5p and 4f levels also interchange along the series. For the lower Z members, like W, the 4f electrons are less tightly bound than the 5p electrons, whereas for the higher Z member Pt it is the other way round. These effects lead to interesting changes in the interactions of ionising photons along the 5d transition metal series, since the $5p \rightarrow 5d$ and $4f \rightarrow 5d$ excitations are strongly coupled to the same $5d \rightarrow \varepsilon f$ continuum. Interest in this series was also stimulated by Boyle et al (1993) who performed detailed calculations of ground state W total and partial photoionization cross sections in the range of the 5p and 4f excitations, using many-body perturbation theory and the relativistic random-phase approximation. Their results suggested a wealth of structures in the photon energy range between 25 and 70eV. In order to probe the correlation effects and to test the theoretical predictions DLP absorption measurements were carried out on atomic W and Pt vapours (Costello et al 1991c). The absorbing vapours were generated by ablation of spectroscopically pure W or Pt targets.

3.6.1.1. Tungsten (W):

For tungsten the power of the dye laser (~1J in 1μs and focal spot size ~ 1mm) was just sufficient to create an absorbing vapour plume. No significant difference was observed between spectra taken at various time delays. This implied that the existence of a significant fraction of W^+ ions could be excluded and that the observed spectrum could be interpreted as due to neutral W. Most of the atoms are probably in the ground state $5p^6 5d^4 6s^2\ ^5D$ but low-lying excited states e.g. $5p^6 5d^5 6s\ ^7S$ may also be populated to some extent.

The relative photoabsorption spectrum of atomic tungsten in the 30 eV to 55 eV range is shown in figure 21. Structures reproduced in a set of spectra are marked and numbered; the corresponding energies are provided in Costello et al (1991c). The calculations by Boyle *et al* showed that the 5p→5d oscillator strength is distributed over a manifold of lines spanning an energy range of approximately 20 eV. In the experimental spectrum two groups of strong lines separated by about 8 eV are clearly discernible. The two dominant peaks are due to the 5p→5d transitions split into two groups by the 5p spin-orbit interaction. The coupling of the 5p→5d resonances to the 5d→εf ionization continua via $5p^5 5d^5 \rightarrow 5p^6 5d^3\ \varepsilon l$ autoionization merges the lines into the broad asymmetric structures displayed by the spectrum. Destructive interference between 5d→εf ionization and 5p→5d excitation results in the pronounced absorption minimum observed at ~32 eV, where the cross section almost goes to zero.

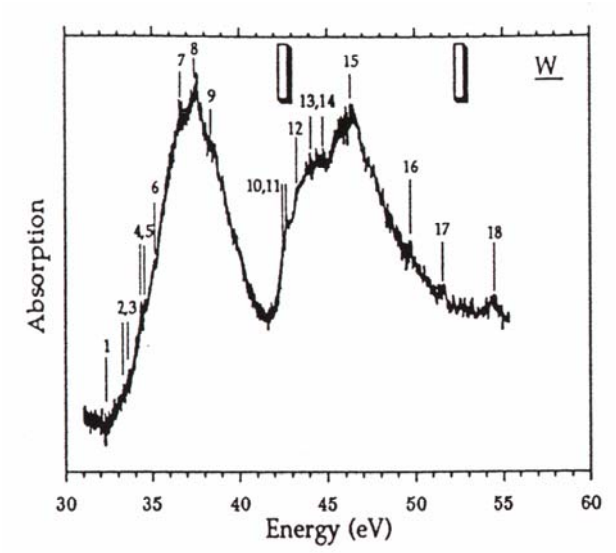

Figure 21. *Relative absorption cross section of W vapour in the photon energy range of the 4f and 5p excitations. Reproducible structures are marked and numbered. The vertical bars mark the positions of the absorption maxima in the spectrum of W metal. See the text for further details. (From Costello et al 1991).*

The total 5d resonant plus the 6s, 4f, 5p and 5s non-resonant cross sections calculations by Boyle et al took relativistic effects and correlations among the $5d^4 \rightarrow 5d^3 \varepsilon l$ channels based on different multiplets of the $5d^3$ ionic core into account. The effect of the strong $5p^6 5d^4 \rightarrow 5p^5 5d^5$ transitions were included as resonant contributions to the 5d partial cross section. The 4f→5d transitions resulted in a series of strong lines at energies between 28 eV and 34 eV in the calculated spectrum. These lines have no counterparts in the experimental spectrum and are therefore expected to lie at energies below the lowest photon energy covered by the spectrum. Weaker 4f→5d lines may be superimposed on the low energy slope of the maximum centred at 37.5 eV. The theory places structures at photon energies approximately 2 eV higher than the corresponding structures in the experiment. If one allows for this energy shift many characteristic features of the experimental spectrum are reproduced by the calculations; e.g. the absorption minimum at 32 eV, the high energy maximum, the shoulder on the low energy side of this maximum and the weak maxima superimposed on its high energy tail. The main difference rests with the strength, energy position and the width of the low energy resonance. The experimental spectrum displays a well-separated resonance centred at 37.5 eV, which comprises an oscillator strength comparable to that of the high energy resonance. There is a low energy resonance at 42 eV in the theoretical spectrum but it is less prominent and contains only a fraction of the strength of the high-energy resonance. The fact that the theory only takes excitations out of the $5d^4 6s^2\ ^5D_0$ ground state into account, whereas excited state absorption contributes to the experimental spectrum, may be one of the reasons for the discrepancy.

The absorption spectrum of W metal (Haensel *et al* 1969, Weaver and Olson 1976) is dominated by two asymmetric resonances, which are similar to those in the atomic spectra. The positions of their maxima, approximately 5 eV above the atomic maxima, are indicated in figure 21. The 5p→5d excitations interacting with the 5d→εl continua are also responsible for the solid-state maxima. It is notable, at the minimum below the 5p transition threshold, the absorption cross section of the metal only drops to about half the peak value, in comparison to the free atom case.

3.6.1.2. Platinum (Pt):

The DLP recorded relative photoabsorption spectrum of atomic Pt in the photon energy range 40 eV to 90 eV is shown in figure 22. The absorbing platinum plume was created by the same long pulse dye laser used for W.

Differences as a function of time delay helped in assigning the Pt features. Structures present only in spectra taken at short time delays are due to transitions from excited states and ions. The spectrum taken at a long time delay of 2.3μs is shown in the figure. The prominent, asymmetric resonance at 50.9 ± 0.2 eV is attributed to $5p_{3/2} \rightarrow 5d$ transitions broadened by the interaction with the $5d \rightarrow \varepsilon f$ autoionization continuum. The asymmetry is caused by the interference of the $5p \rightarrow 5d$ and $5d \rightarrow \varepsilon f$ channels. In contrast to the case of W, the absorption coefficient in the minimum below the 5p onset does not approach zero for Pt. This is due to the stronger $5d \rightarrow \varepsilon f$ continuum and the smaller oscillator strength of the $5p \rightarrow 5d$ transitions. The $5d \rightarrow \varepsilon f$ oscillator strength increases with the number of 5d electrons while the $5p \rightarrow 5d$ oscillator strength decreases with the number of unoccupied 5d levels. The weaker broad maximum at 63.9 ±0.2 eV is ascribed to $5p_{1/2} \rightarrow 5d$ transitions. The energy separation of the two broad resonances, labeled 1 and 2 in the figure, is determined by the 5p spin-orbit splitting. The interaction between the 5p and 5d shells does not cause any further multiple splitting if only $5p^6 5d^9 6s \rightarrow 5p^5 5d^{l0} 6s$ transitions contribute. Due to the near degeneracy of the $5d^9 6s$ and $5d^8 6s^2$ states this simplification does not hold because also $5p^6 5d^8 6s^2 \rightarrow 5p^5 5d^9 6s^2$ excitations have to be taken into account. The assignment of the broad resonances to $5p \rightarrow 5d$ transitions was corroborated by Dirac-Fock calculations performed with the Grant code (Grant *et al* 1980). The calculations yielded two groups of strong lines separated by the spin-orbit splitting of the 5p hole. The vertical bars in figure 22 mark the positions of the $5p \rightarrow 5d$ absorption maxima in the spectrum of Pt metal.

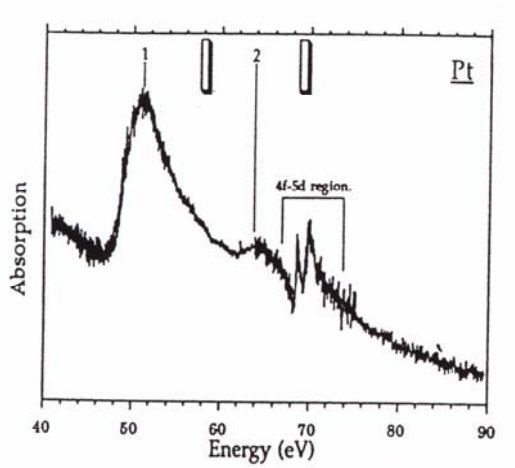

Figure 22. *Relative absorption cross section of Pt vapour in the photon energy range of the 4f and 5p excitations. The vertical bars mark the positions of the absorption maxima in the spectrum of Pt metal. See the text for further details. (From Costello et al 1991c).*

No significant change of the broad resonances (at 50.9 and 63.9 eV) was observed when the time delay between the two DLP laser pulses was varied; in contrast to this the structures around 70 eV, differed considerably for time delays between 0.8 μs and 2.3 μs. The prominent asymmetric resonances remaining at the long time delay (2.3 μs) are assigned to $4f \rightarrow 5d$ excitations according to $(4f^{l4} 5p^6 5d^9 6s + 4f^{l4} 5p^6 5d^8 6s^2) \rightarrow (4f^{l3} 5p^6 5d^{l0} 6s + 4f^{l3} 5p^6 5d^9 6s^2)$ transitions, split by the 4f and 5d spin-orbit interactions and the Coulomb and exchange interactions between the 4f and 5d shells. The resonances are broadened and shifted by the interaction with the $5d \rightarrow \varepsilon f$ ionization continuum and by autoionization and Auger decay channels involving 5p electrons. The strength of the interference effects is illustrated by the Fano type profiles of the resonances. Corresponding peaks are seen in metallic Pt but shifted to higher energies (Haensel *et al* 1969, Dietz *et al* 1980, Williams *et al* 1979).

3.6.2. Photoabsorption by atomic gold:

Lying below one another in the periodic table, Cu (Z=29), Ag (Z=47) and Au (Z=79) are collectively termed the noble metals. The use of gold in many applications e.g. gold coated xuv mirrors, makes it of particular interest for study in this spectral region. In the free atom form, gold has the ground-state configuration $5d^{10} 6s^1$ with a filled 5d subshell, whereas in the metal, 5d hybridization with overlapping 6s and 6p bands leads to a shift of the 5d band in which the hybridized part is located above the Fermi level. Photoabsorption data on free gold atoms from the *valence-excited* state $5d^9 6s^2$ is therefore of interest for comparison with the solid-state spectrum. Furthermore, the configuration of atomic gold in the valence-excited state ($5d^9 6s^2$) means that only a single vacancy exists in the upper electron configuration for $5p \rightarrow 5d$ and $4f \rightarrow 5d$ excitations, which makes gold an interesting member of the heavier elements for the study of electron correlations and relativistic effects. Other phenomena of interest include a cross over of the $5p \rightarrow 5d$ and $4f \rightarrow 5d$ transition lines when following the sequence of 5d transition metals along the periodic table, as mentioned earlier. Gold is the last member of the 5d transition metal series.

The DLP photoabsorption spectrum of Au vapour (Köble et al 1995b) over the 40-110 eV region, recorded at an inter-pulse delay of 600 ns, extends over the 5p and 4f excitation region and is shown in Figure 23. In conjunction with the time resolved photoabsorption study of the Au plasma, a comprehensive set of atomic structure calculations for the main dipole transition lines expected to arise from ground and excited states of the $5d^{10} 6s^1$ and $5d^9 6s^2$ configurations was undertaken. The general shape of the observed spectrum resembles that of Pt except in the energy range of 80 eV, where only one dominant resonance line is observed for gold. The sharp resonance at 80 eV was assigned to the $4f \rightarrow 5d$ transition in *valence-excited* atomic gold according to $4f^{l4} 5d^9 6s^2 (^2D_{5/2}) \rightarrow 4f^{l3} 5d^{l0} 6s^2 (^2F_{7/2})$; the $^2D_{5/2}$ state lies

1.6 eV above the ground state $4f^{l4}5d^{10}6s\ ^2S_{1/2}$ and is metastable in the dipole approximation. The associated $4f^{14}5d^96s^2(^2D_{3/2})$ to $4f^{l3}5d^{l0}6s^2(^2F_{5/2})$ transition was observed at 82 eV particularly at short time delays and as the time delay was increased, reduced in strength compared with the $^2D_{5/2}$ feature. This could be understood in terms of the greater excitation energy (3.0 eV) of the $^2D_{3/2}$ valence-excited level above the ground state. At a time delay of 600 ns (Figure 23), the spectrum is dominated by the $^2D_{5/2}$ feature with only a small hint of the $^2D_{3/2}$ remaining. Therefore the photoabsorption spectrum at 600 ns is expected to arise predominantly from the ground ($^2S_{1/2}$) and valence-excited ($^2D_{5/2}$) states. It proved difficult to record satisfactory spectra for time delays greater than 600 ns as the rapid expansion of the laser plasma plume reduced the optical opacity, resulting in very poor signal to noise ratios. The 600ns spectrum is dominated by the prominent Fano-type resonances attributable to 5p→5d and 4f→5d transitions of valence-excited $5d^96s^2(^2D_{5/2})$ Au, followed by autoionization. The dominant, broad and asymmetric resonance at 55 eV was assigned mainly to the 5p→5d transition from $5p^65d^96s^2(^2D_{5/2}) \rightarrow 5p^55d^{l0}6s^2(^2P_{3/2})$, followed by super Coster-Kronig decay into the $5p^65d^86s^2\ \varepsilon(p,f)$ channels due to the strong overlap between the 5p and 5d orbitals. The interference with the direct 5d photoionisation process is responsible for the asymmetric shape of the resonance. As detailed above, the sharp resonance at 80 eV was assigned to the 4f→5d transition in *valence-excited* atomic gold according to $4f^{l4}5d^96s^2(^2D_{5/2}) \rightarrow 4f^{l3}5d^{l0}6s^2(^2F_{7/2})$. The calculations further showed that the weaker broad resonance at 70 eV could be explained in terms of photoabsorption from the ground state $^2S_{1/2}$ and (to a lesser extent) the $^2D_{3/2}$ valence excited state, followed by a rapid decay, which yields a large peak-width of about 7eV.

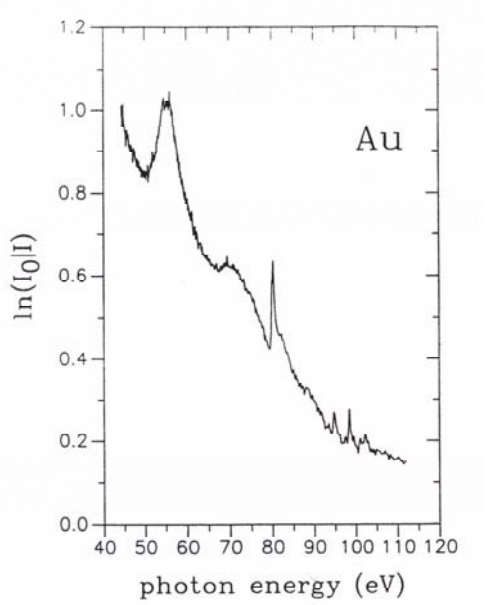

Figure 23. *Relative absorption cross section of Au vapour in the photon energy range of the 4f and 5p excitations. (From Köble et al 1995b).*

In terms of theoretical understanding, the characteristic features in the gold spectrum could be satisfactorily described within the Hartree-Fock theory of resonant photoabsorption taking first-order relativistic corrections into account. Detailed calculations of absolute photoabsorption cross sections of gold from ground and excited states based on the (R)HFand RTDLDA theories were also performed. Interference effects between core and valence-electron excitations manifested in the asymmetric photoabsorption line profiles provided the most significant evidence for electron correlations in gold.

3.6.3. Photoabsorption of the actinides Th and U:

The final examples are from the actinide series. An understanding of the actinides is of fundamental interest and actinide research spans a range of scientific disciplines. Gaining a deeper insight into the physics and chemistry of actinide elements requires understanding the behavior of the 5*f* wave function. With increasing atomic number Z or degree of ionization, the 4*f* wave function in the lanthanides eventually collapses into the inner well see section 3.2), localizing the 4*f* electron which becomes chemically inert. 5*f* electrons in the actinides also experience a double-well potential but do not become localized to the same extent as the 4*f* electrons in the lanthanides due to the additional node in the 5*f* wave function. Many of the physical properties peculiar to the actinides can be attributed to this fact (Haire 1995).

Because of the potential radiological hazards and scarcity of many of the actinides, very few VUV and EUV experiments have been carried out. Thorium and uranium have however been studied with the DLP technique. Carroll and Costello (1986) used the DLP technique to study thorium. In this work they exploited two separate synchronized lasers for the first time. This allowed them to use long inter-plasma time delays and therefore optimize the neutral atomic density. More recently, Meighan et al (1997,2000) used a picosecond laser system to produce a shorter duration backlighting plasma and with the improved temporal resolution obtained the first results for actinide ions by studying the variation in photoabsorption along the thorium isonuclear sequence.

Figure 24 shows some results from a recent extensive study of photoabsorption by atomic uranium in the 15-150 eV region (van Kampen et al 2000). The 6p-subshell photoabsorption behaviour was measured for the first time while

the *5d* region was re-measured using both photoabsorption and photoion spectroscopy. The DLP experiments were performed in the normal incidence (15 –40 eV) and the grazing incidence (30 – 150 eV) regions, covering the 6p and 5d excitation spectral ranges, respectively (Figure 24). The spectra overlapped well in the 30 – 40 eV range, indicating that the VUV and EUV data were obtained under the same experimental conditions. The temperature of the uranium plasma was such that no EUV emission was observed, but in the VUV-DLP experiments corrections to the data were made to take account of a small but detectable emission signal from the absorbing uranium plume. The structures at 21.5 and 30.5 eV (Figure 24) are due to 6p photoabsorption; the peaks at 97.5 and 110 eV result from excitaions from the 5d subshell. In the 40-90 eV region the cross section is smooth, showing no features associated with 6s-subshell photoabsorption.

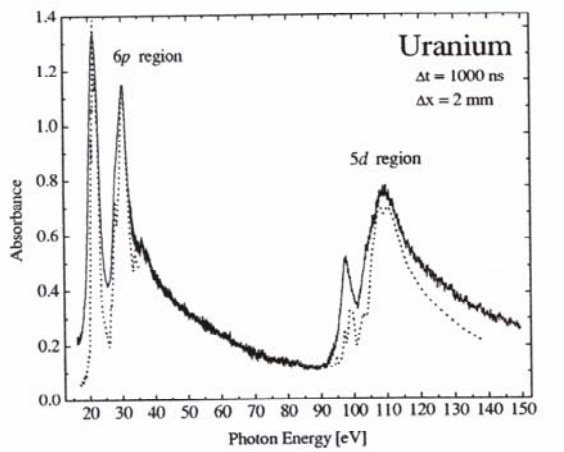

Figure 24. *Experimental (solid line) and calculated (dotted line) photoabsorption spectra of uranium in the 15-150eV region. The calculated spectra have been offset to compensate for the omission of direct photoionization from lower-lying subshells but have not been adjusted otherwise (See text). (From van Kampen et al 2000)*

To interpret the experimental spectra the photoabsorption spectrum of atomic uranium was calculated using the Cowan code (Cowan 1981). As customary in Cowan code calculations, the calculated Slater F_K, G_K and R_k integrals were reduced to 85% of their ab initio values in order to account for interaction with high-lying configurations omitted from the calculation, while the ab initio values of the spin parameter were retained. The calculated spectra for the regions of 6p and 5d photoabsorption are also shown in Figure 24 and compare well with the experimental data. The relative heights of all four experimental peaks are reproduced. Some important conclusions can be drawn from the calculations. The separation of the 6p excitations into two groups of resonances, about 9 eV apart, can be attributed to the spin-orbit splitting of the 6p core hole. The first group of resonances around 21.5 eV can be ascribed to $6p_{3/2} \rightarrow$6d transitions; the second group, around 30 eV, is due to $6p_{1/2} \rightarrow$6d transitions. Both peaks are the result of many unresolved transitions between electrostatically split terms.

In contrast to the 6p case, the two overlapping peaks in the 5d region are not exclusively due to spin-orbit splitting and must be discussed within an intermediate coupling scheme. The calculations reveal that the 5d-5f electrostatic and spin-orbit terms are of comparable importance. Complementary photoion data were obtained in the 80-140 eV region using synchrotron radiation from the electron storage ring BESSY I. The uranium metal was heated in a molybdenum crucible to a temperature of about 2500 K producing an atomic number density in the interaction region $\approx 10^{11}$ cm^{-3}. The photoion experiments provided individual yields for U^+, U^{2+} and U^{3+} ions over the 5d excitation regime. No U^{4+} ions were detected. Figure 25 shows the individual yields and a comparison of the summed photoion yield and the DLP photoabsorption data. The latter agree very well and provide a check on the reliability of the experimental results.

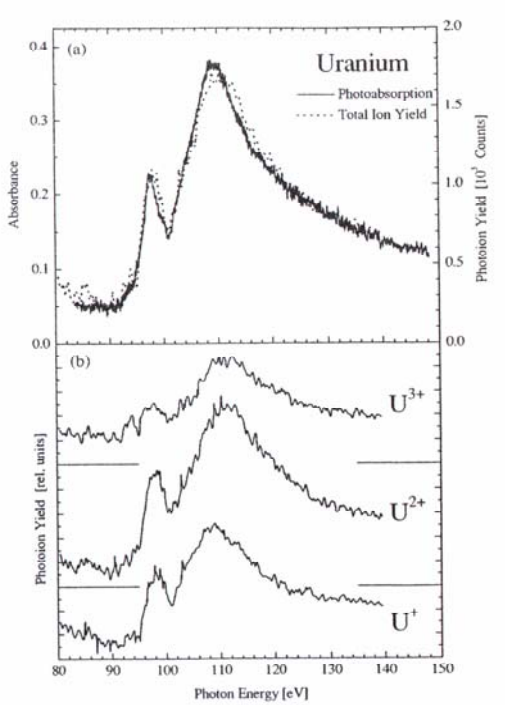

Figure 25. *Experimental photoabsorption and photoion yield spectra of atomic uranium in the 5d region: (a) summed photoion yield and photoabsorption spectra; (b) individual U^+, U^{2+}, and U^{3+} photoion yields. (From van Kampen et al 2000)*

The photoabsorption spectra of thorium and uranium (Carroll and Costello 1986, 1987) are quite similar in appearance: the 6p photoabsorption spectrum of thorium exhibits the same distinct spin-orbit splitting into two peaks centered at photon energies of 20.6 and 27.2 eV. Thorium has atomic number Z=90 and a ground-state configuration [Rn] $5f^0 6d^2 7s^2$, and yet the center of the uranium $6p_{3/2} \rightarrow 6d$ resonance lies only 1-eV higher than that of thorium, indicating that in going from thorium to uranium, the increase in core charge is almost entirely compensated for by the shielding effect of the 5f electrons. Further details on the extensive calculations for uranium and the comparison with the experimental results may be obtained in van Kampen et al (2000).

4. Future perspectives:

4.1. Laser plasma light source developments

Efforts are continuing to improve laser plasmas as light sources for short wavelength spectral regions. Most of the DLP experiments to date have used nanosecond laser systems to produce the backlighting continuum. Recent efforts (Meighan et al 1997, 2000) to generate shorter duration backlighting pulses, by using picosecond laser systems, have proved successful in improving the temporal resolution obtainable in DLP experiments. This can be particularly helpful when higher ion stages are to be isolated, as the temporal discrimination required is greater than when lower ion stages are explored.

In DLP experiments on atoms and ions it is usual to allow the backlighting continuum to pass through the absorbing plasma plume before dispersion by the spectrometer system (see Figure 1 and 2). This has the advantage of providing a wide spectral capture, ideal for investigating spectral structures the exact energies of which are not usually known beforehand. By placing a spectrometer between the backlighting source and the absorbing plasma plume a monochromatized beam may be generated. This has recently been achieved (Hirsch et al 2000, 2003) with a system based on a 1m normal incidence vacuum monochromator with corrected (toroidal) optics that produces a wavelength tuneable and collimated vacuum-ultraviolet (30 – 100 nm) beam. The VUV continuum source is a laser generated gold plasma. The primary function of the system is the measurement of time resolved 'images' or spatial distributions of photoabsorption/photoionization in expanding plasma plumes.

In microelectronics photolithography processing there is a continuing search for efficient light sources at shorter and shorter wavelengths, in order to overcome diffraction imposed limitations to feature size. If laser plasmas are to be serious contenders for EUV photolithography sources then they need to be optimized for a wavelength of 13.5 nm while at the same time substantially improving their emission efficiencies and reducing the debris emitted (Dunne et al 2000, de Bruijn et al 2003). This remains a major challenge.

4.2. Synchrotron developments

The first successful photoion spectrometry experiment carried out with merged synchrotron radiation and an ion (Ba^+) beam was accomplished at the Daresbury storage ring (Lyon et al 1986). In subsequent experiments other singly charged ions Ca^+, S^+, Ga^+ and Zn^+ were studied in this way. All the measurements involved resonantly enhanced cross sections. Only for K^+ was it possible to measure the near threshold non-resonant photoionisation cross section (Peart and Lyon 1987). While only moderate spectral resolution was achieved in these early experiments, the most

important and pioneering aspect of these experiments was that they provided absolute values of the cross sections. Over the last five years or so, improvements in storage ring light sources and the installation of ion sources on beamlines at SuperACO (Paris), Astrid (Aarhus), Photon Factory (Tsukuba) and ALS (Berkeley) have resulted in absolute cross sections being determined for many additional ions, both singly and multiply charged, including several of strong astrophysical significance (West 2001, 2002). In photoion experiments, the ion yields in different charged channels provides a measure of the corresponding cross sections (see e.g. Figure 25). The LURE group at Orsay has recorded multiply charged results including the Ba isonuclear sequence (Bizau et al 2001). The Aarhus group has achieved results for a wide range of ions, many of astrophysical interest, mostly for singly (Kjeldsen et al 1999a,b, 2000) but including a few doubly charged species. The highest spectrally resolved results for ions have been achieved at the Advanced Light Source (ALS), the third generation storage ring at Berkeley (Aguilar et al 2003). As an example, Figure 26 shows the photoionisation absolute cross section for Sc^{2+} ions at about 40 eV where the resonant structures have been scanned with a spectral bandwidth of only 1.2 meV (Schippers et al 2003). It is clear that these storage ring based facilities will continue over the next few years to add to the growing database of photoionisation cross sections for both positively and negatively charged ions and will provide important benchmark measurements for the evaluation of appropriate theoretical approximations.

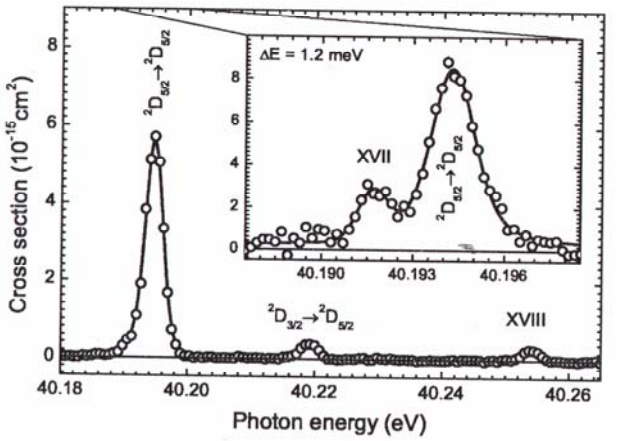

Figure 26. *Measured (open symbols) and fitted (full line) photoionisation cross section in the region of the Sc^{2+} $3p^63d^2\ ^2D\rightarrow 3p^53d^62(^3F)\ ^2D$ resonances measured with high resolution at the Advanced Light Source storage ring photoion facility. The inset shows the maximum energy resolution achieved of 1.2 meV, corresponding to a resolving power E/ΔE of 33,500. (From Schippers et al 2003)*

Synchrotron radiation experiments on neutral atoms are however still far ahead of the corresponding situation for ions. Prepared in well defined ground or excited states, often oriented or aligned, neutral atoms have been subjected to spectroscopies such as photoabsorption, fluorescence, photoion and photoelectron techniques, which have provided detailed partial cross sections, the angular distribution of emitted electrons and spin/polarization parameters of single and multiple ionization processes. In comparison, photoelectron spectroscopy experiments with ion beams are still in their infancy. The first photoelectron spectroscopy experiment with an ion beam was carried out at SuperACO (Bizau et al 1991). The experiment was extremely difficult due to the inherent low efficiency of the electron spectrometer (~1%) compared to an ion spectrometer (~100%) and the shorter photo-ion interaction region (~1cm) compared with that in photoion experiments (typically 10 – 20 cm). Furthermore the density of an ion beam is much less than that achievable in a neutral atomic beam. In order to detect the emitted electrons, the very strongly resonantly enhanced cross section associated with the 3p→3d resonance of Ca^+ was exploited. More recent developments (still relying on the 2000Mb Ca^+ resonance) resulted in greater sensitivity and the first angular resolved measurements (AlMoussalami et al 1996). If electron spectrometry of ions is ever to become routine this will require much higher photon fluxes than currently achievable at third generation storage rings.

4.3. VUV Free Electron Laser (FEL) developments

Attainment of the long sought after goal of tunable laser-like radiation in the VUV and EUV spectral regions is now becoming a reality with the construction of single-pass Free Electron Lasers (FELs) based on the principle of Self Amplified Spontaneous Emission (SASE). VUV FELs will provide uniquely intense, polarised, short pulse (<~100fs) and tunable coherent radiation.

In a SASE FEL kinetic energy of a highly-relativistic electron bunch from a linear accelerator is converted to coherent electromagnetic radiation. Lasing occurs in a single pass of the electron bunch through a long (~30m) ultra-precise magnetic undulator. The alternating magnetic field of the undulator permanent magnetic structure forces the electrons to oscillate sideways and therefore emit electromagnetic radiation wavepackets, which are extremely strongly peaked in the forward direction in the laboratory frame of reference. The emitted electromagnetic radiation interacts with the electron bunch leading to a density modulation (micro-bunching - with a spacing equal to the wavelength) which enhances the power and coherence of the radiation emitted by the bunch. *This process of self-amplification leads to exponential growth of the radiation field and to saturated laser-quality output.* The emission wavelength is given by $\lambda_n = \lambda_u(1+K^2/2)/2n\gamma^2$ where λ_u is the period length of the undulator (typically cms), $\gamma = E/mc^2$ is the relativistic factor of the electrons and the undulator parameter $K = eB_0\lambda_u/2\pi mc$ where B_o is the peak magnetic field in the undulator. Because λ_u is of the order of cms (2.7 cm at DESY) and γ is of the order of 2000 for a 1Gev accelerator, the FEL emission wavelength λ_n is extremely short. The wavelength can be most readily tuned by varying

the energy of the electrons from the accelerator.

The FEL preferentially builds up the em wave at λ_n as this wavelength is resonant for the undulator. As an electron propagates through the undulator the lightwave that it emits travels at speed c. In each period of the undulator the relativistic electron slips behind with respect to its emitted light by λ_n so that the waves emitted by an individual electron, as a result of each sideways oscillation, add coherently. The induced microbunching builds up a coherence between the electromagnetic waves emitted by different electrons in the bunch. The combination of the two effects leads to the unique and unprecedented nature of the final output beam brilliance.

While similar in many ways to the undulator beamlines of existing third generation storage rings the key aspects that make SASE FELS at short wavelengths achievable, are the unprecedented quality of the electron bunches, which need to be highly monoenergetic and of very low emittance, and the demands placed on the accelerator technologies and the precision and scale of the overall accelerator/undulator system. The German research centre DESY (Hamburg) is currently developing the world's first Free Electron Laser to operate at short wavelengths (Feldhaus 2001, Sonntag 2001, Kennedy 2000). A decisive milestone was achieved in February 2000 when the first coherent output from the Phase 1 DESY FEL was observed (Andruszkow et al 2000). By 2001 the FEL produced the first saturated output and achieved GW pulses in the femtosecond regime (Ayvazyan et al 2002).

The first scientific results obtained with the DESY Phase 1 FEL were reported by Wabnitz et al (2002) and involved the interaction of the VUV photons (at ~ 90nm) with xenon atoms and clusters. These are essentially the first results on the interaction of intense VUV light with matter. The time-of-flight mass spectra of the ionization products are shown in Figure 27, as a function of cluster size. Whereas the Xe atoms only became singly ionized by the absorption of single photons, the absorption in clusters was strongly enhanced. On average, each atom in large clusters absorbed up to 400 eV, corresponding to 30 photons. It was suggested that the clusters are heated up and electrons are emitted after acquiring sufficient energy, the clusters finally disintegrating completely by Coulomb explosion. The behaviour was strikingly different to that which occurs with intense optical laser light.

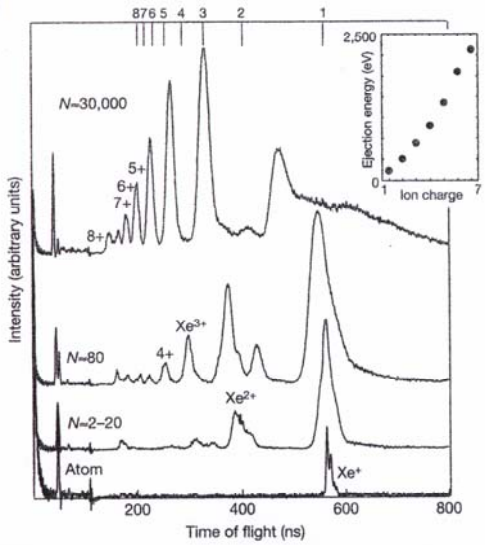

Figure 27. *Time-of-flight (TOF) mass spectra of ionization products of Xe atoms and clusters recorded after ionization with radiation at 98 nm from the DESY Free Electron Laser, with an average power density of 2 x 10^{13}W cm^{-2}. N is the number of atoms per cluster. Whereas only singly charged ions are observed after irradiation of isolated atoms, atomic ions with charges up to 8^+ are detected if clusters are irradiated. The inset shows the kinetic energy of the ions as a function of the charge for a cluster with 1,500 atoms. (From Wabnitz et al 2002)*

The Phase I FEL was shut down in 2002 in order to facilitate the next phase of development. A full-scale VUV-FEL facility, including a new experimental hall and infrastructure to direct the FEL beam into different beamlines, is expected to become operational as a user facility in 2004. The Phase 2 FEL accelerator will be capable of reaching 1GeV and will produce photon wavelengths ranging down to 6 nm. Ultimately the average values of brilliance and photon flux will be more than three orders of magnitude higher than those provided by the current most advanced third generation storage rings e.g. achievable by BESSY II (Berlin) or the Advanced Light Source (Berkeley) synchrotron storage rings; the peak values are expected to be more than nine orders of magnitude higher!! *Such FEL lasers will constitute scientific investigative tools of dramatically new capability.* Moving to very short wavelengths places extreme demands on the qualities of the accelerators and undulators required. Nevertheless, DESY (Hamburg) and SLAC (Stanford) have planned projects to develop SASE FELs aimed at eventually producing photon beams with tunable wavelengths stretching through the water window ($2.4 \leq \lambda \leq 4.4$nm; important in many biological applications) down to wavelengths of the order of ~ 0.1/0.2nm – the natural dimension of atoms, molecules and material interatomic spacings (Rossbach 1996, Tatchyn et al 1996). (See also the DESY TESLA Design Report: ISBN 3-935702-04-3: available on the Web at www.desy.de).

Studies of atom and ion interactions with the intense FEL photon beam will be of fundamental interest. Atoms constitute perfectly regenerative targets making them extremely suitable for early investigations. Additionally, such

experiments can provide data of importance for the interpretation of FEL beam interactions with the corresponding atomic species in cluster or solid matrices. The super-intense output of the FEL will enable completely new physical regimes for the interaction of radiation with atoms to be explored. Moderate focusing of the VUV-FEL output will produce peak power densities sufficiently high to enable new VUV *non-linear* phenomena to be studied. FEL experiments on atoms and ions will result in new insights into the interaction of intense VUV/EUV radiation with matter. They will also provide important diagnostic data and benchmark measurements for future FEL developments. The high flux photon beam will allow very low cross section atomic processes or very dilute beams (such as prepared ion beams) to be explored, including electron spectroscopy investigations. The high intensities achievable will allow single versus multi-photon processes to be compared. Synchronizing the FEL with other lasers will enable sub-picosecond pump-probe experiments. In anticipation of the FEL several calculations have been carried out on the interaction of intense short wavelength radiation with atoms. These include hydrogen (Bauer et al 2001), helium (Hasbani et al 2000, Kornberg and Lambropoulos 1999, Dundas et al 1999, Saenz and Lambropoulos 1999) and multi-electron atoms (Brewczyk and Rzazewski 2001, Novikov and Hopersky 2000)

5. Conclusion

Over the last forty years or so major progress has been possible in the study of the interaction of ionizing radiation with atoms and ions, due to developments in lasers, detectors and synchrotron radiation facilities. The Dual Laser Plasma technique has proved flexible in terms of its ability to investigate atoms and ions of a wide range of elements. Investigations of trends in the photoabsorption behaviour along isoelectronic and isonuclear sequences, have led to many new results. Inner-shell and multiple-electron processes have been explored. Following initial pioneering investigations in the late eighties, the use of storage ring radiation in conjunction with ion beams has been reinvigorated over the last five years or so and photoion yield experiments at several large scale synchrotron facilities are now providing absolute cross section results both positive and negative ions. While many of the results to date are for singly charged species, this situation is changing and multiply charged positive ions are now also subject to investigation. With the advent of the SASE Free Electron Laser providing access to unprecedented intensities at large photon energies it is anticipated that the interaction between photon beams and free atoms and ions at short wavelengths will become an area of even more intense research in the coming years. The large-scale synchrotron or FEL facilities operate in energy scanning mode and, particularly when high spectral resolution is sought, require prior information on energies and relative cross sections of spectral structures, if efficient use is to be made of limited beam-times. The Dual Laser Plasma technique has the advantage of being fairly readily applied to different elements and will continue to provide early exploratory measurements of atomic and ionic processes, interesting in their own right and useful precursors to later more detailed investigations with either synchrotron or FEL sources.

Acknowledgements

The authors wish to thank their many collaborators (including in particular former PhD students A. Gray, L. Kiernan, U. Koble, O. Meighan, W. Whitty and post-doctoral researchers A. Neogi and C. McGuinness) who have contributed to the results reviewed here. We also express our appreciation to the various funding agencies who have made it possible over the years for us to engage in this research. These include Enterprise Ireland, the EU, the Higher Education Authority and Dublin City University. We thank Sheila Boughton for her help in the preparation of the manuscript.

References

Adam, M.Y.A., Stranges, S., de Simone, M., Svensson, S. and Combet-Farnoux, F. (1994) Coster-Kronig decay of 3p core-excited states of atomic zinc. *Phys. Rev. A* **49**, 1797.

Aguilar, A., West, J.B., Phaneuf, R.A., Broder, R.L., Folkmann, F., Kjeldsen, H., Bozek, J.D., Schlachter, A.S. and Cisneros, C. (2003) Photoionization of isoelectronic ions: Mg^{+} and Al^{2+}. *Phys. Rev. A* **67**, 012701-1/8.

AlMoussalami, S., Bizau, J.M., Rouvellou, B., Cubaynes, D., Journel, J., Wuilleumier, F.J., Obert, J., Putaux, J.C., Morgan, T.J., Richter, M. (1996) First angle-resolved photoelectron measurements following inner-shell resonant excitations in a singly charged ion. *Phys. Rev. Lett.* **76**, 4496-4499.

Andruszkow, J. et al. (2000) First observation of self-amplified spontaneous emission in a free-electron laser at 109nm wavelength. *Phys. Rev. Lett.* **85**, 3825.

Ayvazyan, V. et al. (2002) Generation of GW radiation pulses from a VUV free-electron laser operating in the femtosecond regime. *Phys. Rev. Lett.* **88**, 104802-1-4.

Azuma, Y., Koike, F., Cooper, J.W., Nagata, T., Kutluk, G., Shigemasa, E., Wehlitz, R., Sellin, I.A. (1997) Photoexcitation of hollow lithium with completely empty *K* and *L* shells. *Phys. Rev. Lett.* **79**, 2419-2422.

Azuma, Y., Hasegawa, S. , Koike, F., Kutluk, G., Nagata, T., Shigemasa, E., Yagishita, A., Sellin, A. (1995) New photon-induced triply excited hollow atom states of lithium. *Phys. Rev. Letter* **74,** 3678.

Ballofet, G., Romand, J. and Vodar B. (1961) Emission source of continuous spectra extending from the visible to the far ultraviolet. *Compt. Rend.* **252**, 4139.

Bauer, J., Plucinski, L., Piraux, B., Potvliege, R., Gajda, M., Krzywinski, J. (2001) Interaction of hydrogen atoms by intense vacuum ultraviolet radiation. *J. Phys. B: At. Mol. Opt. Phys.* **34**, 2245-2254.

Beutler, H. (1935) *Z. Astrophys.* **93**, 177.

Bizau, J.M., Cubaynes, D., Esteva, J.M., Wuilleumier, F.J., Blancard, C., Bruneau, J., Champeaux, J.P., La Fontaine, A.C., Couillaud, C., Marmoret, R., Remond, C., Hitz, D., Delaunay, M., Haque, N., Deshmukh, R.C., Zhou, H.L., Manson, S.T. (2001) Absolute measurements and theoretical calculations of photoionization cross-sections along the isonuclear sequence of multiply charged barium ions. *Phys. Rev. Lett.* **87**, 273002.

Bizau, J.M., Cubaynes, D., Richter, M., Wuilleumier, F.J., Obert, J., Putaux, J.C., Morgan, T.J., Kallne, E., Sorenson, S. and Damany, A. (1991) 1st Observation of Photoelectron Spectra Emitted in the Photoionization of a Single-Charged Ion Beam with Synchrotron Radiation. *Phys. Rev. Lett.* **67**, 576-579.

Boyle, J., Altun, Z. and Kelly, H.P. (1993) Photoionization cross-section calculation of atomic tungsten. *Phys. Rev. A* **47**, 4811-4830.

Brewczyk, M. and Rzazewski, J. (2001) Interaction of multi-electron atom with intense radiation in the VUV range: beyond the conventional model for high harmonic generation. *J. Phys. B: At. Mol. Opt. Phys.* **34**, L289-L296.

Cantu, A.M. and Tondello, G. (1975) Continuum source and focusing technique for the 80-500 Angstrom spectral range: Improvements. *Appl. Opt.* **14**, 996-998.

Carillon, A., Jaegle, P. and Dhez, P. (1970) Extreme ultraviolet continuum absorption by a laser generated aluminium plasma. *Phys. Rev. Lett.* **25**, 140-143.

Carroll, P.K. and Costello, J.T. (1986) Giant-dipole-resonance in atomic thorium by a novel two-laser technique. *Phys. Rev. Lett.* **57**, 1581-3.

Carroll, P.K. and Costello, J.T. (1987) The XUV photoabsorption spectrum of uranium vapour. *J. Phys. B: At. Mol. Opt. Phys.* L201-L205.

Carroll, P.K. and Kennedy, E.T. (1977) Doubly excited autoionisation resonances in the absorption spectrum of Li^{+} formed in a laser-produced plasma. *Phys. Rev. Lett.* **38**, 1068-1071.

Carroll, P.K., Kennedy, E.T. and O'Sullivan, G. (1978) New continua for absorption spectroscopy from 40 to 2000 Angstroms. *Opt. Lett.* **2**, 72-74.

Carroll, P.K., Kennedy, E.T. and O'Sullivan, G. (1980) Laser-produced continua for absorption spectroscopy in the VUV and XUV. *Appl. Opt.* **19**, 1454-1462.

Carroll, P.K. and O'Sullivan, G. (1982) Ground state configurations of ionic species I through XVI for Z=57-74 and the

interpretation of 4d-4f emission resonances in laser produced plasmas. *Phys. Rev. A.* **25**, 275-286.

Chakraborty, H.S., Gray, A., Costello, J.T., Deshmukh, P.C., Haque, G.N., Kennedy, E.T., Manson, S.T., Mosnier, J-P. (1999) Anomalous behavior of the near-threshold photoionization cross section of the neon isoelectronic sequence: A combined experimental and theoretical study. *Phys. Rev. Lett.* **83,** 2151-2154.

Cheng, K.T. and Froese Fischer, C. (1983) Collapse of 4f orbital for Xe-like ions. *Phys. Rev. A* **28**, 2811-1819.

Cheng, K.T. and Johnson, W.R. (1983) Orbital collapse and the photoionization of the inner 4d shells. *Phys. Rev. A* **28**, 2820-2828.

Chung, K.T. (1998) Photoionization of lithium from the $1s^2 2p$ state. *Phys. Rev. A* **57**, 3518-3522.

Chung, K.T. (1999) Auger decay of multiply excited atomic systems. *Phys. Rev. A* **59**, 2065-2070.

Chung, K.T. and Gou, B. (1995) Energies and lifetimes of triply excited states of lithium. *Phys. Rev. A* **52**, 3669-3676.

Chung, K.T. and Gou, B. (1996) High $^2P^o$ resonances of a triply excited lithium atom. *Phys. Rev. A* **53**, 2189-2193.

Clark, C.W. and Greene, C.H. (1980) Hyperspherical analysis of three-electron dynamics. *Phys. Rev. A* **21**, 1786.

Codling, K. (1973) Applications of synchrotron radiation (ultraviolet spectral light source). *Reps. Prog. Phys.* **36**, 541.

Codling, K. and Madden, R.P. (1972) Resonances in the photoionization continuum of Kr and Xe. *J. Res. Nat. Bur. Std.* Sect. **A76**, 1.

Conneely, M.J. and Lipsky, L. (2002) Energy levels and classifications of triply excited states of Li, Be^+, B^{2+} and C^{3+}. *At. Data and Nucl. Data Tables* **82,** 115-190.

Connerade, J.P., Esteva, J.M. and Karnatak, R.C.(1987) Eds: Giant Resonances in Atoms, Molecules and Solids. (Plenum Press, New York)

Connerade, J.P. and Lane A.M. (1987) The interaction between a Rydberg series and a shape or giant resonance. *J. Phys. B: At. Mol. Opt. Phys.* **20**, L181-6.

Connerade, J.P. and Mansfield, M.W.D. (1974) Structure in the Zn I absorption spectrum associated with the excitation of the $3s^2$ subshell. *Proc. R. Soc. A* **339**, 533.

Cooper, J.W., Fano, U. and Prats, F. (1963) Classification of two-electron excitation levels of helium. *Phys. Rev. Lett.* **10**, 518-521.

Costello, J.T., Mosnier, J-P, Kennedy, E.T., Carroll, P.K. and O'Sullivan, G. (1991a) XUV absorption spectroscopy with laser-produced plasmas: A Review. *Phys. Scripta* **J34**, 77-92.

Costello, J.T., Kennedy, E.T., Sonntag, B.F. and Clark, C.W. (1991b) 3p-subshell absorption spectra of free and bound Cr, Cr^+, Mn and Mn^+. *Phys. Rev. A* **43**, 1441.

Costello, J.T., Kennedy, E.T., Sonntag, B.F. and Cromer, C.L. (1991c) XUV photoabsorption of laser generated W and Pt vapours. *J. Phys. B: At. Mol. Opt. Phys.* **24**, 5063.

Cowan, R.D. (1981) The Theory of Atomic Structure and Spectra. (Berkeley, CA: Univ. of California Press).

Cubaynes, D., Diehl, S., Journel, L., Rouvellou, B., Bizau, J.-M., Moussalami, S. Al., Wuilleumier, F.J., Berrah, N., VoKy, L., Faucher, P., Hibbert, A., Blancard, C., Kennedy, E.T., Morgan, T.J., Bozek, J. and Schlachter, A.S. (1996) First photoexcitation measurements and *R*-matrix calculations of even-parity hollow states in laser-excited lithium atoms. *Phys. Rev. Lett.* **77**, 2194-2197.

De Bruijn, R., Koshelev, K., Kooijman, G., Toma, E.S., Bijkerk, F. (2003) Absorption of EUV in laser plasmas generated on xenon gas jets. *J.Quant.Spectr. & Rad.Transfer* **81**, 97-105.

Diehl, S., Cubaynes, D., Bizau, J.-M., Journel, L., Rouvellou, B., Moussalami, S.Al., Wuilleumier, F.J., Kennedy, E.T., Berrah, N., Blancard, C., Morgan, T.J., Bozek, J., Schlachter, A.S., VoKy, L., Faucher, P. and Hibbert, A. (1996) High resolution measurements of partial photoionization cross sections in hollow lithium: A critical comparison with advanced many-body calculations. *Phys. Rev. Lett.* **76**, 3915-3918.

Diehl, S., Cubaynes, D., Wuilleumier, F.J., Bizau, J-M, Journel, L., Kennedy, E.T., Blancard, C., VoKy, L., Faucher, P., Hibbert, A., Berrah, N., Morgan, T.J., Bozek, J. and Schlachter, A.S. (1997a) Experimental observation and theoretical calculations of the lowest doubly hollow lithium state. *Phys. Rev. A. Rapid Comm.* **56**, R1071-1074.

Diehl, S. Cubaynes, D., Wuilleumier, F.J., Bizau, J.M, Journel, L., Kennedy, E.T., Blancard, C., VoKy, L., Faucher, P., Hibbert, A., Berrah, N., Morgan, T.J., Bozek, J. and Schlachter, A.S. (1997b) Experimental observation and theoretical calculations of Rydberg series in hollow lithium atomic states. *Phys. Rev. Lett.* **79**, 1241-1244.

Diehl, S., Cubaynes, D., Kennedy, E.T., Wuilleumier, F.J., Bizau, J-M, Journel, L., VoKy, L., Faucher, P., Hibbert, A., Blancard, C., Berrah, N., Morgan, T.J., Bozek, J. and Schlachter, A.S. (1997c) Hollow-atom - hollow-ion decay routes of triply excited lithium: First Auger results and a comparison with R-matrix calculations. *J. Phys. B: At. Mol. Opt. Phys.* **30**, L595-L605.

Diehl, S., Cubaynes, D., Bizau, J-M, Wuilleumier, F.J., Kennedy, E.T., Mosnier, J-P and Morgan, T.J. (1999) New high-resolution measurements of doubly excited states of Li^+. *J. Phys. B: At. Mol. Opt. Phys.* **32**, 4193-4207.

Diehl, S., Cubaynes, D., Zhou, H.L., VoKy, L., Wuilleumier, F.J., Kennedy, E.T., Bizau, J.M., Manson, S.T., Morgan, T.J., Blancard, C., Berrah, N. and Bozek, J. (2000a) Angle-resolved photoelectron spectrometry studies of the autoionization of the $2s^2 2p$ triply excited state of atomic lithium: Experimental results and R-matrix calculations. *Phys. Rev. Lett.* **84**, 1677-1680.

Diehl, S., Cubaynes, D., Zhou, H.S., VoKy, L., Wuilleumier, F.J., Kennedy, E.T., Bizau, J.M., Manson, S.T., Blancard, C., Berrah, N. and Bozek, J. (2000b) The $2p^3$ triply excited hollow resonance of lithium: measurement and calculation of partial cross sections and angular behaviour. *J. Phys. B: At. Mol. Opt. Phys.* **33**, L487-L494.

Dietz, R.E., McRae, E.G. and Weaver, J.H. (1980) Core-electron excitation edges in metallic Ni, Cu, Pt and Au. *Phys. Rev. B* **21**, 2229-2247.

Dolmatov, V.K. (1996) First theoretical study of the 3p absorption cross section of free Cr^+. *J. Phys. B: At. Mol. Opt. Phys.* **29**, L673-6.

Donnelly, D., Bell, K.L. and Hibbert, A. (1997) Breit-Pauli R-matrix calculation of the 3p photoabsorption of single ionized chromium. *J. Phys. B: At. Mol. Opt. Phys.*
30, L285-91.

Dundas, D., Taylor, K.T., Parker, J.S. and Smyth, E.S. (1999) Double-ionization dynamics of laser-driven helium. *J. Phys. B: At. Mol. Opt. Phys.* **32**, L231-L238.

Dunne, P. O'Sullivan, G. and Ivanov, V.K. (1993) Extreme ultraviolet absorption spectrum of Ga^+. *Phys. Rev. A* **48**, 4358-4364.

Dunne, P., O'Sullivan, G. and O'Reilly, D. (2000) Prepulse-enhanced narrow bandwidth soft x-ray emission from a low-debris, subnanosecond laser plasma light source. *Appl. Phys. Lett.* ***76****, 34-36.*

Edlen, B. (1942) Interpretation of the emission lines in the spectrum of the solar corona. *Z. Astrophys.* **20**, 30-64.

Edlen, B. (1964) Wavelength measurements in the vacuum ultraviolet. *Reps. Prog. Phys.* (IOP and Physics London) Vol **26**, 181.

Fawcett, B.C., Gabriel, A.H., Irons, F.E., Peacock, N.J. and Saunders, P.A.H. (1966) Extreme ultra-violet spectra from laser-produced plasmas. *Proc. Phys. Soc.* **88**, 1051-1053.

Feldhaus, J. (2001) Status and perspectives of single pass free electron lasers for short wave lengths. *J. de Physique* I*V***, 11**, 237-244.

Gabriel, A.H. (1970) Plasma Light Sources. *Nucl. Instr. Meth.* **90**, 157.

Garton, W.R.S. (1966) Spectroscopy in the Vacuum Ultraviolet (Eds. D.R. Bates and I. Estermann, Academic, New York) Vol 2, 93-176

Garton, W.R.S., Connerade, J.P., Mansfield, M.W.D. and Wheaton, J.E.G. (1969) Atomic absorption spectroscopy in the 100-600 Å wavelength range. *Applied Optics* **8**, 919-924.

Grant, I.P., McKenzie, B.J., Norrington, P.H., Mayers, D.F. and Pyher, N.C. (1980) An atomic multiconfigurational Dirac-Fock package. *Comput. Phys. Commun.* **21**, 207-231.

Gray, A. (1999) PhD Thesis. XUV photoabsorption studies of calcium and the neon isoelectronic sequence. Dublin City Unversity.

Greene, C.H. and Clark, C.W. (1984) Adiabatic hyperspherical treatment of lithium $^2P^0$ states , *Phys. Rev. A* **30**, 2161.

Grujic, P.V. (1999) Triply excited three-electron systems semi classical model. *Eur. Phys.* **D 6,** 441-450.

Haensel, R., Radler, K., Sonntag, B. and Kunz, C. (1969) Optical absorption measurements of tantalum, tungsten, rhenium and platinum in the extreme ultraviolet. *Solid State Comm*. **7**, 1495-1497.

Haire, R.G. (1995) Comparison of the chemical and physical properties of f-element metals and oxides – their dependence on electrical properties. *J. Alloys.Compd.* **223**, 185-196.

Hartman, P.L., and Tomboulian, D.H. (1953) Far ultraviolet radiation from the Cornell synchrotron. *Phys. Rev.* **91**, 1577-1578.

Hasbani, R., Cormier, E. and Bachau, H. (2000) Resonant and non-resonant ionization of helium by XUV ultrashort and intense laser pulses. *J. Phys. B: At. Mol. Opt. Phys.* **33**, 2101-2116.

Hibbert, A. and Scott, M.P. (1994) Atomic data for opacity calculations 21 the neon sequence. *J. Phys. B: At. Mol. Opt. Phys.* **27**, 1315-1323.

Hirsch, J.S., Meighan, O., Mosnier, J.P., van Kampen, P., Whitty, W. W., Costello, J. T., Lewis, C. L. S., MacPhee, A. G., Hirst, A. G., Westhall, J. and Shaikh, W. (2000) Vacuum ultraviolet resonant photoabsorption imaging of laser produced plasmas. *J.Appl. Phys.* **88**, 4953-60.

Hirsch, J.S., Kennedy, E.T., Neogi, A. and Costello, J.T. (2003) Vacuum-ultraviolet photoabsorption imaging system for laser plasma plume diagnostics. *Rev. Sci. Instrum.* **74**, 2992-2998.

Hopfield, J.J. (1930) Absorption and emission spectra in the wavelength region 600-1100A^{o}. *Phys.Rev.* **35**, 1133-1134.

Jannitti, E., Nicolosi, P. and Tondello, G. (1984) Photoionisation and double excitation spectrum of Be^{2+}. *Opt. Commun.* **50**, 225-30.

Jannitti, E., Nicolosi, P. and Tondello, G. (1990) Absorption spectra from 1s inner-shell electron of ionized and neutral carbon. *Physica Scripta* **41**, 458-463.

Kennedy, E.T. (2000) Looking at the bright side of VUV SASE FELS. *Nucl. Instr. Meth. A* **445/1-3**, 463.

Kennedy, E.T. (2001) Photogeneration of hollow atoms: Recent developments. *Physica Scripta* **T95**, 32-42.

Kennedy, E.T., Costello, J.T. and Mosnier, J-P. (1995) Inner shell photoionization of atoms, excited atoms and ions with laser generated plasmas. *Proc. 4th US-Mexico Symposium on Atomic and Molecular Physics*, Eds. C Cisneros and T J Morgan (World Scientific Publishers) p406-423.

Kennedy, E.T., Costello, J.T., Mosnier, J-P, Cafolla, A.A., Collins, M., Kiernan, L., Köble, U., Sayyad, M.H. and Shaw, M. (1994) Extreme ultraviolet studies with laser produced plasmas. *Opt. Eng* **33**, 3964-3992.

Kennedy, E.T., Costello, J.T., Mosnier, J-P, van Kampen, P. (2001) Atomic and ionic photoionization data for astrophysics: Applications of the dual laser plasma technique. *Spectroscopic Challenges of Photoionized Plasmas*, APS Conference Series, (Eds: G Ferland & D Savin) p127-132

Kennedy, E.T., Diehl, S., Cubaynes, D., Bizau, J-M. and Wuilleumier, F.J. (1998) Photonic, electronic and atomic collisions. (Edited by F. Aumayr and H. Winter) (World Scientific: Singapore 1998) p.129

Kiernan, L.M., Costello, J.T., Kennedy, E.T., Mosnier, J-P and Sonntag, B.F. (1997) Measurement of the XUV photoabsorption spectra of atomic zinc and its ions Zn^{m+}: m=1,2&3 in the region of 3p subshell excitation. *J. Phys. B: At. Mol. Opt. Phys.* **29**, 4801-4812.

Kiernan, L.M., Lee, M-Q, Sonntag, B.F., Sladeczek, P., Zimmermann, P., Kennedy, E.T., Mosnier, J-P and Costello, J.T. (1995) High resolution photoion yield spectrum of 'hollow' atomic lithium. *J. Phys. B: At. Mol. Opt. Phys*. **28**, L161-L168.

Kiernan, L., Mosnier, J-P, Kennedy, E.T., Costello, J.T. and Sonntag, B.F. (1994) First observation of a photon induced triply excited state in atomic lithium. *Phys. Rev. Lett.* **72**, 2359-2362.

Kjeldsen, H., Folkmann, F., Hansen, J.E., Knudsen, H., Rasmussen, M.S., West, J.B. and Andersen, T. (1999a) Measurement of the absolute photoionization cross-section of C^{+} near threshold. *Astrophys.J.* **524**, L143-L146.

Kjeldsen, H., Folkmann, F., Knudsen, H., Rasmussen, M.S. West, J.B. and Andersen, T. (1999b) Absolute photoionization cross-section of K^{+} ions from the 3p to the 3s threshold. *J. Phys. B: At. Mol. Opt. Phys.* **32**, 4457-4465.

Kjeldsen, H., West, J.B., Folkmann, F., Knudsen, H. and Andersen, T. (2000) The absolute photoionization cross section of singly charged ions in the extreme ultraviolet. *J. Phys. B: At. Mol. Opt. Phys.* **33**, 1403-1414.

Köble, U. (1994) Ph.D. Thesis A photoabsorption study of La^{3+} and Au in the giant resonance energy region , Dublin City University

Köble, U., Kiernan, L., Costello, J-T, Mosnier, J-P, Kennedy, E.T., Ivanov, V.K., Kupchenko, V.A. and Shendrik, M.S. (1995a) Observation of a 4f(^{1}P) Giant Dipole Resonance in La^{3+}. *Phys. Rev. Lett* **74**, 2188.

Köble, U., Costello, J.T., Mosnier, J-P, Kennedy, E.T. and Martins, M. (1995b) XUV photoabsorption of laser generated Au vapour. *J. Phys. B: At. Mol. Opt. Phys.* **28**, 181-190.

Kornberg, M.A. and Lambropoulos, P. (1999) Photoelectron energy spectrum in 'direct' two-photon double ionization of helium. *J. Phys. B: At. Mol. Opt. Phys.* **32**, L603-L613.

Lagutin, B.M., Demekhin, Ph.V., Petrov, I.D., Sukhorukov, V.L., Lauer, S., Liebel, H., Volliveiler, F., Schmoranzer, H., Wilhelmi, O., Mentzel, G. and Schartner, K-H (1999) Photoionization of Ar and Ar-like ions near the 3s-threshold. *J. Phys. B: At. Mol. Opt. Phys.* **32**, 1795-1807.

Lucatorto, T.B., McIlrath, T.J., Sugar, J. and Younger S.M. (1981) Radical redistribution of the 4d oscillator strengths observed in the photoabsorption of the Ba, Ba^+ and Ba^{2+} sequence. *Phys. Rev. Lett.* **47**, 1124.

Lyman, T. (1924) *Astrophys.J.* **60**, 1.

Lyman, T. (1928) The Spectroscopy of the Extreme Ultraviolet. (Longmans, Green New York, 2nd Ed.).

Lyon, I.C., Peart, B., West, J.B. and Dolder, K. (1986) Measurements of absolute cross-sections for the photoionization of Ba^+ ions. *J. Phys. B: At. Mol. Opt. Phys.* **19**, 4137-4147.

Madden, R.P. and Codling, K. (1963) New autoionizing atomic energy levels in He, Ne and Ar. *Phys. Rev. Lett.* **10**, 516-518.

Mansfield, M.W.D. and Audley, M.D. (2003) Private Communication.

Mansfield M.W.D., Costello, J.T., Kennedy, E.T. and Mosnier, J-P. (2003) The 4p-subshell photoabsorption spectrum of singly ionised molydenum. *J. Phys. B: At. Mol. Opt. Phys*. **36** 2611-2628.

McGuinness, M., Martins, M., van Kampen, P., Hirsch, J., Kennedy, E.T., Mosnier, J-P, Whitty, W.W. and Costello, J.T. (2000) Vacuum-UV absorption spectrum of a laser produced chromium plasma: 3p-subshell photoabsorption by Cr^{2+} ions. *J. Phys. B: At. Mol. Opt. Phys*. **33**, 5077 –5090.

McGuinness, C., Martins, M., Wernet, Ph., Sonntag, B.F., van Kampen, P., Mosnier, J-P, Kennedy, E.T., and Costello, J.T., 1999, Metastable state contributions to the measured 3p photoabsorption spectrum of Cr^+ ions in a laser-produced plasma , *J. Phys. B: At. Mol. Opt. Phys.* **32** L583-L591

McGuire, J.H., Berrah, N., Barlett, R.J., Samson, J.A.R., Tanis,J.A., Cocke, C.L., Schlachter, A.S. (1995) The ratio of cross-sections for double to single ionization of helium by high energy photons and charged particles *J. Phys. B: At. Mol. Opt. Phys.* **28**, 913-940.

Meighan, O., Dardis, L., Kennedy, E.T., Morgan, T.J., Mosnier, J-P, van Kampen, P.and Costello, J.T. (1997) Observation of a 6p-6d giant dipole resonance in the VUV photoabsorption spectrum of a laser-produced thorium plasma. *J. Phys. B: At. Mol. Opt. Phys.* **32** L285-L290.

Meighan, O., Danson, C., Dardis, L., Lewis, C.L.S., MacPhee, A., McGuinness, C., O'Rourke, R., Shaikh, W., Turcu, I.C.E. and Costello, J.T. (2000) Application of a picosecond laser plasma continuum light source to a dual-laser plasma photoabsorption experiment. *J. Phys. B: At. Mol. Opt. Phys.* **33**, 1159-1168.

Millikan, R.A. and Bowen, I.S. (1924) Extreme ultra-violet spectra. *Phys. Rev.* **23**, 1-34.

Millikan, R.A. and Sawyer, R.A. (1918) Extreme ultra-violet spectra of hot sparks in high vacuum. *Phys. Rev.* **12**, 167-170.

Morishita, T. and Lin, C.D. (1999) Comprehensive analysis of electron correlations in three-electron atoms. *Phys. Rev. A*. **59**, 1835-1843.

Morishita, T. Tolstikhin, O.I., Watanabe, S. and Matsuzawa, M. (1997) Hyperspherical hierarchy of three-electron radial excitations. *Phys. Rev. A.* **56**, 3559-3568.

Mosnier, J-P, Costello, J.T., Kennedy, E.T. and Whitty, W.W. (2000) The photoabsorption spectrum of laser generated Li^+ in the 60 eV to 180 eV photon energy range. *J. Phys. B: At. Mol. Opt. Phys.* **33**, 5203 – 5214.

Mosnier, J-P, Sayyad, M.H., Costello, J.T., Kiernan, L. and Kennedy, E.T. (1994) Even parity autoionising states of Mg, Al^{+} and Si^{2+} in the extreme ultraviolet. *Phys. Rev. A*. **49**, 755-761.

Neogi, A., Kennedy, E.T., Mosnier, J-P, van Kampen, P., O' Sullivan, G., Mansfield, M.W.D., Demekhin, Ph. V., Lagutin, B.M., Petrov, I.D., Sukhorukov, V.L. and Costello, J.T. (2003) Trends in autoionisation of Rydberg states converging to the 4s threshold in the Kr – Rb+-Sr^{2+} - Y^{3+} series: Experiment and theory. *Physical Review A.* **67**, 042707-1-10.

Nicolosi, P. and Villoresi, P. (1998) Experimental measurement of the CII L-shell photoabsorption spectrum. *Phys. Rev. A.* **58**, 4985-4988.

Novikov, S.A. and Hopersky, A.N. (2000) Two-photon excitation/ionization of atomic inner shells. *J. Phys. B: At. Mol. Opt. Phys.* **33**, 2287-2294.

Olsen, C.G. and Lynch, D.W. (1982) Rare-earth 4d absorption spectra in rare-earth triflorides. *J. Opt. Soc. Am.* **72**, 88.

Osgood, T.H. (1927) X-Ray Spectra of Long Wave-Length. *Phys. Rev.* **30**, 567-573

Peart, B. and Lyon, I.C. (1987) Measurements of absolute photoionization cross-sections of K^{+} ions. *J. Phys. B: At. Mol. Opt. Phys.* **20**, L673.

Rau, A.R.P. (1992) Excitation and decay of correlated atomic states. *Science* **258**, 1444-1451.

Recanatini, P., Nicolosi, P.and Villoresi, P. (2001) ^{2}P and ^{4}P CII photoabsorption spectra. *Phys Rev A*. **64,** 012509-1/10.

Richardson, M. (2000) In "Vacuum Ultraviolet Spectroscopy". Eds: J A Samson and D L Ederer (Academic Press) p. 83-92.

Rossbach, J. (1996) A VUV free electron laser at the TESLA test facility at DESY. *Nucl. Instr. and Meth.* **A 375**, 269-273.

Saenz, A. and Lambropoulos, P. (1999) Theoretical two-, three- and four-photon ionization cross section of helium in the XUV range. *J. Phys. B: At. Mol. Opt. Phys.* **32**, 5629-5637.

Samson J.A.R. (1967) Techniques of Vacuum Ultraviolet Spectroscopy. (Wiley & Sons)

Samson J.A. and Ederer, D.L. (2000) Vacuum Ultraviolet Spectroscopy. (Eds: Academic Press ISBN: 0-12-617560-8).

Schmidt, V. (1997) Electron Spectrometry of Atoms using Synchrotron Radiation. (Cambridge Uni. Press, ISBN: 0 521 55053).

Schippers, S., Müller, A., Ricz, S., Bannister, M.E., Dunn, G.H., Schlach ter, A.S., Hinojosa, G., Cisneros, C., Aguilar, A., Covington, A.M., Gharaibeh, M.F. and Phaneuf, R.A. (2003) Photoionization of Sc^{2+} ions by synchrotron radiation: Measurements and absolute cross sections in photon energy range 23-68eV. *Phys. Rev. A*. **67**, 032710-1/13.

Schulz, K., Kaindl, G., Domke, M., Bozek, J. D., Heimann, P. A., Schlachter, A. S. and Rost, J. M. (1996) Observation of new Rydberg series and resonances in doubly excited helium at ultrahigh resolution. *Phys. Rev. Lett.* **77**, 3086-3089.

Schumann, V. (1893) *Akad. Weiss. Wein.* **102**, 625.

Schwinger, J. (1949) On the classical radiation of accelerated electrons. *Phys. Rev.* **75**, 1912-1925.

Sonntag, B. (2001) VUV and X-ray free electron lasers. *Nucl. Instr. Meth. A* **467** Part 1, 8-15.

Sonntag, B.F. and Zimmerman, P.(1992) XUV spectroscopy of metal atoms. *Rep. Prog. Phys.* 911.

Speer, R. J. (1972) Some recent aspects of spectroscopy at UV and X-ray wavelengths in Atoms and Molecules in Astrophysics (Eds. Carson, T. R. and Roberts, M. J. Academic Press ISBN 0-12-161050-0) p285-310

Tatchyn, R., Arthur, J., Baltay, M., Bane, K., Boyce, R., Cornacchia, M., Cremer, T., Fisher, A., Hahn, S.J., Hernandex, M., Low, G., Miller, R., Nelson, W.R., Nuhn, H.D., Palmer, D., Paterson, J., Raubenheimer, T., Weaver, J., Wiedemann, H., Winick, H., Pellegrini, C., Travish, G., Scharlemann, E.T. Caspi, S., Fawley, W., Halbach, K., Kim, K.J., Schlueter, R., Xie, M., Meyerhofer, D., Bonifacio, R., DeSalvo, L., (1996) Research and development toward a 4.5-1.5 Angstrom linear coherent light source (LCLS) at SLAC. *Nucl. Instr. and Meth.* **A 375**, 274-283.

Tomboulian, D.H. and Hartman, P.L. (1956) Spectral and angular distribution of ultraviolet radiation from the 300-Mev Cornell synchrotron. *Phys.Rev.* **102**, 1423-1447.

Tousey, R. (1962) *Appl. Opt.* **1**, 679.

Ullrich, J., Moshammer, R., Dorner, R., Jagutzki, O., Mergal, V., SchmidtBocking, H. and Spielberger, L. (1997) Recoil-ion momentum spectroscopy. *J. Phys. B: At. Mol. Opt. Phys.* **30**, 2917-2974.

van Kampen, P., O'Sullivan, G., Ivanov, V.K., Ipatov, A.N., Costello, J.T. and Kennedy, E.T. (1997) Dramatic changes in the 3s autoionization process at the beginning of the Ar I sequence. *Phys. Rev. Lett*. **78**, 3082-3085.

van Kampen, P., Gerth, Ch., Martins, M., Carroll, P.K., Hirsch, J., Kennedy, E.T., Mosnier, J-P, Zimmermann, P. and Costello, J.T. (2000) Photoabsorption and photoion spectroscopy of atomic uranium in the region of 6p and 5d excitations. *Phys. Rev. A*. **61**, 2706 – 2712.

Verbockhaven, G. and Hansen J.E. (2000) Autoionization of triply excited Rydberg series. *Phys. Rev. Lett.* **84**, 2810-2813.

Wabnitz, H. et al. (2002) Multiple ionization of atom clusters by intense soft X-rays from a free electron laser. *Nature* **420**, 482-485.

Weaver, J.H. and Olson, G.G. (1976) Optical absorption in the 4d transition metals from 20 to 250 eV. *Phys. Rev. B*. **14**, 3251-3255.

Weidemann, H. (2003) Synchrotron Radiation (Springer-Verlag, ISBN 3540433929)

Wehlitz, R., Huang, M.T., DePaola, B.D., Levin, J.C., Sellin, I.A., Nagata, T., Cooper, J.W. and Azuma, Y. (1998) Triple photoionization of lithium. *Phys. Rev. Lett.* **81**, 1813-1816.

Wehlitz, R., Pattard, T., Huang, M.-T., Sellin, I.A., Burgdörfer, J., Azuma, Y. (2000) Near-threshold triple-photoionization cross section of lithium. *Phys. Rev. A*. **61**, 030704®.

West, J.B. (2001) Photoionization cross sections of atomic ions. *J. Phys. B: At. Mol. Opt. Phys.* **34**, R45-R91.

West, J.B. (2002) Photoionization cross sections of atomic ions. *J. Electr. Spectros. & Rel. Phen.* **123**, 247-256.

Williams, G.P., Lapeyre, G.J., Anderson, J., Dietz, R.E. and Yafet, Y. (1979) 4f core threshold effects in photoemission from Pt. *J. Vac. Sci. Technol.* **16**, 528-530.

Wuilleumier, F.J., Diehl, S., Cubaynes, D., Bizau, J.-M. and Kennedy, E.T. (1998) Photoelectron spectroscopy studies of hollow lithium states. *J. of Elec. Spec. Rel. Phen.* **41**, 88-91.

Wuilleumier, F.J. (2000) From doubly excited states of helium to triply excited states of lithium. *Phys. Essays* **13**, 230-247 special issue.